Cancer cells differentially modulate mitochondrial respiration to alter redox state and enable biomass synthesis in nutrient-limited environments

Sarah M. Chang[1,2], Muhammad Bin Munim[1,2], Sonia E. Trojan[1,3], Anna Shevzov-Zebrun[1,2], Keene L. Abbott[1,2], and Matthew G. Vander Heiden[1,2,4*]

[1]Koch Institute for Integrative Cancer Research, Massachusetts Institute of Technology, Cambridge, MA, USA

[2]Department of Biology, Massachusetts Institute of Technology, Cambridge, MA, USA

[3]Jagiellonian University Medical College, Faculty of Medicine, Chair of Medical Biochemistry, Krakow, Poland

[4]Dana-Farber Cancer Institute, Boston, MA, USA

*Correspondence: mvh@mit.edu

Abstract

The cell NAD+/NADH ratio can constrain biomass synthesis and influence proliferation in nutrient-limited environments. However, which cell processes regulate the NAD+/NADH ratio is not known. Here, we find that some cancer cells elevate the NAD+/NADH ratio in response to serine deprivation by increasing mitochondrial respiration. Cancer cells that elevate mitochondrial respiration have higher serine production and proliferation in serine limiting conditions than cells with no mitochondrial respiration response, independent of serine synthesis enzyme expression. Increases in mitochondrial respiration and the NAD+/NADH ratio promote serine synthesis regardless of whether serine is environmentally limiting. Lipid deprivation can also increase the NAD+/NADH ratio via mitochondrial respiration in some cells, including cells that do not increase respiration following serine deprivation. Thus, in cancer cells where lipid depletion raises the NAD+/NADH ratio, proliferation in serine depleted environments improves when lipids are also depleted. Taken together, these data suggest that changes in mitochondrial respiration in response to nutrient deprivation can influence the NAD+/NADH ratio in a cell-specific manner to impact oxidative biomass synthesis and proliferation. Given the complexity of tumor microenvironments, this work provides a metabolic framework for understanding how levels of more than one environmental nutrient affects cancer cell proliferation.

Introduction

Rapidly proliferating cells, including cancer cells, must acquire biomass precursors such as amino acids, lipids, and nucleotides to support cell growth and division (Deberardinis, 2008; Faubert, 2020; Hanahan, 2011; Pavlova, 2017; Vander Heiden, 2017). While cells can obtain biomass precursors from the environment, many tissue and tumor environments can be deficient in necessary nutrients (Cognet, 2024; Gullino, 1964; Lyssiotis, 2017). In these conditions, cells depend on biosynthesis to accumulate sufficient biomass for proliferation (Apiz Saab, 2023; Ferraro, 2021; Ngo, 2020; Sciacovelli, 2022; Sullivan, 2019b; Sullivan, 2019a). Synthesis of many

48 biomass precursors involve oxidation reactions, which require the redox cofactor NAD+ to act as
49 an electron acceptor. There is accumulating evidence that NAD+ availability and the cell redox
50 state (NAD+/NADH ratio) can limit the synthesis of biomass precursors, including aspartate
51 (Birsoy, 2015; Sullivan, 2015), asparagine (Krall, 2021), fatty acids (Li, 2022), serine (Baksh, 2020;
52 Bao, 2016; Broeks, 2023; Diehl, 2019), and nucleotides (Bao, 2016; Diehl, 2019; Wu, 2024). Thus,
53 the NAD+/NADH ratio impacts cancer cell proliferation in nutrient environments that increase the
54 dependence on biosynthetic oxidation reactions. However, what determines the cellular
55 NAD+/NADH ratio and whether the NAD+/NADH ratio is modulated in response to environmental
56 nutrient availability is not well characterized. Moreover, whether differences in the NAD+/NADH
57 ratio across cell types affect sensitivity to different nutrient limitations is not known.

58 Some tumor microenvironments have low levels of serine, an amino acid used to produce
59 many biomass components, including proteins, nucleotides, glutathione, and lipids. Thus, low
60 serine environments can limit cancer cell proliferation and tumor growth (Banh, 2020; Maddocks,
61 2013; 2017; Ngo, 2020; Sullivan, 2019b). In serine depleted environments, cancer cells must
62 increase serine synthesis to maintain proliferation (DeNicola, 2015; Labuschagne, 2014;
63 Locasale, 2011; Possemato, 2011; Sullivan, 2019b). Serine synthesis involves the conversion of
64 the glycolytic intermediate 3-phosphoglycerate (3-PG) into serine. The production of 3-PG from
65 glucose involves an oxidation reaction catalyzed by glyceraldehyde 3-phosphate dehydrogenase
66 (GADPH). 3-PG is then oxidized by phosphoglycerate dehydrogenase (PHGDH) in the first step
67 of the serine synthesis pathway. Both GADPH and PHGDH require NAD+ as an electron acceptor
68 to enable serine synthesis. Experimentally suppressing NAD+ regeneration from NADH
69 decreases serine synthesis, which can be rescued by oxidizing the NAD+/NADH ratio via
70 exogenous electron acceptor supplementation (Bao, 2016; Diehl, 2019; Gravel, 2014). Similarly,
71 *de novo* fatty acid synthesis can be constrained by the NAD+/NADH ratio, as the production of
72 fatty acids involves multiple oxidation reactions to generate citrate from either glucose or
73 glutamine. Thus, decreasing the NAD+/NADH ratio sensitizes cells to environmental lipid

depletion (Li, 2022). Together, these findings demonstrate that exogenous changes to the NAD+/NADH ratio can alter serine and citrate production and impact proliferation in serine or lipid-depleted environments. However, auxotrophy for a single nutrient is not sufficient to determine whether cancer cells can form tumors in a tissue, where levels of multiple nutrients may be environmentally limiting for proliferation (Abbott, 2024; Sivanand, 2024; Sullivan, 2019a).Thus, we aimed to uncover how the endogenous NAD+/NADH ratio of cancer cells is regulated to influence biosynthesis in different nutrient depleted environments and its role in determining cancer cell proliferation when multiple oxidized nutrients are limiting.

By culturing cancer cells in serine depleted conditions and examining the relationship between the NAD+/NADH ratio and serine synthesis, we find that the NAD+/NADH ratio is elevated in response to serine deprivation in some but not all cancer cells. The elevated NAD+/NADH ratio is driven by increased mitochondrial respiration and promotes serine synthesis to confer resistance to environmental serine depletion. A similar relationship between mitochondrial respiration and the NAD+/NADH ratio was observed in lipid-depleted environments, where higher mitochondrial respiration in some cells led to elevated NAD+/NADH ratios and enhanced citrate synthesis. Lastly, we find that any perturbation that increases the NAD+/NADH ratio, including either serine or lipid deprivation, led to both elevated serine and citrate production, regardless of what nutrient was depleted from the environment. Together, these data reveal that the NAD+/NADH ratio is regulated by mitochondrial respiration in response to environmental nutrients in a cancer cell-specific manner and that this influences oxidative biosynthesis and proliferation. These data also provide insight into how levels of multiple nutrients in tissue microenvironments may cooperate to enable biomass synthesis and cell proliferation. This study is based in part on work performed for a PhD dissertation (Chang, 2024).

Results

Modulating the cell NAD+/NADH ratio proportionally alters serine synthesis

100 To begin investigating the processes that determine the cell NAD+/NADH ratio and
101 influence biomass synthesis, we examined the relationship between the NAD+/NADH ratio and
102 serine synthesis in serine replete and serine limited conditions. Previous studies have found that
103 decreasing the cell NAD+/NADH ratio (more reduced) can suppress serine production (Baksh,
104 2020; Bao, 2016; Broeks, 2023; Diehl, 2019). To confirm this, we varied the cell NAD+/NADH
105 ratio upon serine withdrawal and measured the serine synthesis rate of A549 non-small cell lung
106 cancer cells, which transcriptionally upregulate the serine synthesis enzyme PHGDH (DeNicola,
107 2015). We increased the NAD+/NADH ratio by treating cells with the exogenous electron acceptor
108 alpha-ketobutyrate (AKB), which can be reduced to alpha-hydroxybutyrate to regenerate NAD+
109 (Sullivan, 2015) (**Figure 1A**). We decreased the NAD+/NADH ratio by treating cells with rotenone,
110 an inhibitor of mitochondrial complex I, which regenerates NAD+ in support of respiration. AKB
111 and rotenone dose-dependently increased and decreased the cell NAD+/NADH ratio, respectively
112 (**Figure 1B**). To measure the serine synthesis rate in cells, we performed kinetic isotope tracing
113 using uniformly ^{13}C-labeled glucose (U-^{13}C-glucose) and measured production of M+3 labeled
114 serine (**Figure 1C**). Because intracellular serine, including newly synthesized serine, rapidly
115 exchanges with the serine-free extracellular environment (Labuschagne, 2014), we collected both
116 media and cells to ensure detection of all newly synthesized serine produced from glucose. We
117 find that increasing the cell NAD+/NADH ratio with AKB led to proportionally higher serine
118 synthesis rates whereas lowering the cellular NAD+/NADH ratio with rotenone led to
119 proportionally lower serine synthesis rates (**Figure 1D**). This was not explained by changes in
120 PHGDH protein expression, as altering the NAD+/NADH ratio with AKB or rotenone did not affect
121 PHGDH protein levels despite modulating serine synthesis (**Supplementary Figure 1A,B**). Of
122 note, we find that serine synthesis rate is positively correlated with the cell NAD+/NADH ratio
123 (**Figure 1E**). Accordingly, the NAD+/NADH ratio is also positively correlated with proliferation rate
124 following serine depletion (**Figure 1F,G; Supplementary Figure 1C**). Together, these data

125 demonstrate that modulating the NAD+/NADH ratio leads to proportional changes in serine
126 synthesis rates and proliferation in serine-depleted environments.
127
128 **Cancer cells with elevated NAD+/NADH ratios following serine withdrawal exhibit greater**
129 **serine synthesis**
130 Based on our finding that the NAD+/NADH ratio correlates with serine synthesis rate, we
131 wondered whether endogenous cell NAD+/NADH ratios, which differ across cancer cells, are
132 predictive of proliferation rate following serine deprivation. To test this, we measured how
133 proliferation rate varied in a panel of cancer cells derived from various tissues-of-origin and with
134 different genetic driver mutations, and found a wide range of sensitivity to serine deprivation
135 (**Figure 2A**, **Supplementary Figure 2A, Supplementary Table 1**). Because PHGDH expression
136 is important for proliferation in serine depleted conditions (DeNicola, 2015; Locasale, 2011;
137 Maddocks, 2017; Possemato, 2011; Sullivan, 2019b), we first assessed PHGDH protein
138 expression across the different cancer cells to examine how well this explained environmental
139 serine dependence. As expected, some cells with low PHGDH protein expression (MCF7, MDA-
140 MB-231) were most sensitive to serine withdrawal, and some cells with higher PHGDH protein
141 levels were more resistant to serine withdrawal (PHGDH-overexpressing MDA-MB-231, A375)
142 (**Supplementary Figure 2A-C**). However, for many cancer cells PHGDH expression alone could
143 not fully explain sensitivity to serine withdrawal (**Supplementary Figure 2D**). For example, when
144 comparing the non-small cell lung cancer cells A549 and H1299, H1299 cells express less
145 PHGDH protein than A549 cells but are more resistant to serine deprivation **(Supplementary**
146 **Figure 2B-D)**. Consistent with lower PHGDH protein expression, H1299 cells express lower
147 levels of NRF2, a transcriptional regulator of serine biosynthesis enzymes, including PHGDH
148 (DeNicola, 2015). Importantly, A549 and H1299 cells proliferate similarly in serine replete
149 conditions (A549: 1.17 doublings per day; H1299: 1.33 doublings per day), arguing that
150 differences in basal proliferation cannot explain the different sensitivities to serine depletion

151 (**Supplementary Figure 2A**). Given the finding that the NAD+/NADH ratio correlates with serine
152 synthesis rate, we hypothesized that differences in the NAD+/NADH ratio upon serine deprivation
153 could contribute to the variability in sensitivity to serine withdrawal across cells with similar
154 PHGDH protein levels (Calu6, A549, PaTu8988T, MIA PaCa-2, H1299, and HCT116)
155 (**Supplementary Figure 2B-D**). To test this, we measured the cell NAD+/NADH ratios in the
156 presence and absence of exogenous serine. Interestingly, we find that serine starvation elevated
157 the NAD+/NADH ratio in some cells, while minimally changing the NAD+/NADH ratio in others
158 (**Figure 2B, Supplementary Figure 2E**). Strikingly, cells with elevated cell NAD+/NADH ratios
159 following serine withdrawal were more resistant to serine depletion compared to cells with
160 unchanged NAD+/NADH ratios (**Figure 2C**). The NAD+/NADH ratio was also elevated in cancer
161 cells with higher PHGDH protein levels upon serine depletion (A375, PHGDH-overexpressing
162 MDA-MB-231) (**Supplementary Figure 2B,E**). To confirm that an elevated NAD+/NADH ratio in
163 response to serine depletion was associated with elevated serine synthesis, we compared how
164 serine synthesis rates changed following serine withdrawal in A549 and H1299 cells. Indeed, in
165 serine depleted conditions, H1299 cells demonstrated a higher rate of serine synthesis, a larger
166 increase in serine synthesis, and had higher serine levels than A549 cells, consistent with the
167 elevated NAD+/NADH ratio in H1299 cells (**Figure 2D,E; Supplementary Figure 2F,G**). Taken
168 together, these data suggest that in some cells, the cell NAD+/NADH ratio is responsive to serine
169 availability and increases in the NAD+/NADH ratio correlate with increased serine synthesis and
170 proliferation rates in serine-depleted conditions independent of PHGDH protein expression.
171

172 **Increased mitochondrial respiration is associated with an elevated NAD+/NADH ratio and**
173 **increased serine synthesis**

174 The finding that some cancer cells exhibit a more oxidized NAD+/NADH ratio upon serine
175 starvation is surprising, particularly when increased serine synthesis will result in a higher demand
176 for NAD+ to support increased flux through GAPDH and PHGDH (Diehl, 2019; Maddocks, 2017).

177 We hypothesized that the elevated NAD+/NADH ratio represented a cellular response to make
178 the NAD+/NADH ratio more oxidized to enable serine synthesis and thus sought to identify the
179 processes that led to the increased NAD+/NADH ratio in some but not all cancer cells. Lactate
180 production via lactate dehydrogenase (LDH) is a major NAD+ regenerating process, particularly
181 in cancer cells with high glucose fermentation (Fantin, 2006; Luengo, 2021; Wang, 2022)
182 (**Supplementary Figure 3A**); however, lactate secretion relative to glucose consumption was not
183 elevated following serine deprivation in any cells tested (**Supplementary Figure 3B**).
184 Mitochondrial respiration is another major way cells regenerate NAD+ from NADH (Handy, 2012).
185 Thus, we tested whether changes in mitochondrial respiration, as measured by cellular oxygen
186 consumption, accompany the increase in NAD+/NADH ratio following serine withdrawal. Indeed,
187 cells that increased their NAD+/NADH ratio following serine deprivation also exhibited increased
188 rates of oxygen consumption, whereas cells with unaltered NAD+/NADH ratios following serine
189 withdrawal did not (**Figure 3A, Supplementary Figure 3C**). To test whether elevated oxygen
190 consumption was related to serine deprivation, we cultured H1299 and A549 cells in varying
191 amounts of extracellular serine and measured oxygen consumption rates. Oxygen consumption
192 of A549 cells was not impacted by varying extracellular serine levels, while oxygen consumption
193 of H1299 cells increased as extracellular serine decreased below 100 μM, the serine
194 concentration where proliferation begins to be affected most by serine limitation (**Figure 3B,**
195 **Supplementary Figure 3D**). The increase in oxygen consumption rate also corresponded with
196 the NAD+/NADH ratio in H1299 cells at different serine levels, while the NAD+/NADH ratio in
197 A549 cells was unchanged by extracellular serine availability (**Figure 3C, D).** Consistently, the
198 NAD+/NADH ratio in H1299 cells cultured in different concentrations of serine positively
199 correlated with serine synthesis, whereas A549 cells displayed minimal changes in serine
200 synthesis rate (**Figure 3E, F**). Notably, PHGDH protein levels remained constant as extracellular
201 serine levels were decreased in both A549 and H1299 cells (**Supplementary Figure 3E**).
202 Together, these findings suggest that increased NAD+/NADH ratios in response to decreasing

203 environmental serine are linked to elevated mitochondrial respiration in select cancer cells, and
204 that this enables increased serine synthesis.
205
206 **Mitochondrial respiration governs the cell NAD+/NADH ratio and influences serine**
207 **synthesis rate**
208 To test whether increased mitochondrial respiration following serine depletion causes an
209 increase in the cell NAD+/NADH ratio, we treated redox unresponsive cells (i.e. cells that do not
210 elevate oxygen consumption or the NAD+/NADH ratio following serine withdrawal) with the proton
211 ionophore carbonyl cyanide-4-(trifluoromethoxy)phenylhydrazone (FCCP), which
212 pharmacologically increases mitochondrial oxygen consumption by uncoupling respiration from
213 ATP synthesis (McLaughlin, 1980; Terada, 1990). Increasing respiration with FCCP elevates
214 mitochondrial NAD+ regeneration and the cell NAD+/NADH ratio (Luengo, 2021) (**Figure 4A**).
215 Indeed, FCCP treatment dose-dependently improved proliferation of redox unresponsive cells in
216 serine-depleted conditions (**Figure 4B, Supplementary Figure 4A**). In contrast, FCCP did not
217 improve the proliferation of redox responsive cells grown without serine (**Figure 4C,**
218 **Supplementary Figure 4B**). Consistent with its impact on proliferation, FCCP treatment led to
219 higher serine synthesis rates only in redox unresponsive A549 cells while having no impact on
220 the serine synthesis rates of redox responsive H1299 cells (**Figure 4D,E, Supplementary Figure**
221 **5A-D**). As expected, uncoupling mitochondrial respiration from ATP synthase with FCCP led to
222 elevated oxygen consumption in serine depleted A549 cells (**Figure 4F).** FCCP also increased
223 oxygen consumption in serine depleted H1299 cells (**Supplementary Figure 4C**). Interestingly,
224 FCCP raised the NAD+/NADH ratios of both A549 and H1299 cells following serine withdrawal
225 despite only improving serine synthesis and proliferation in A549 cells (**Figure 4G,**
226 **Supplementary Figure 4D**). The lack of impact on serine synthesis by FCCP in H1299 cells
227 suggests that NAD+ availability may not further constrain serine synthesis in cells that already
228 elevate mitochondrial respiration following environmental serine depletion. In this context, we

229 considered whether another constraint such as PHGDH protein expression was limiting serine
230 synthesis in redox responsive cells treated with FCCP. Indeed, overexpressing PHGDH in serine-
231 depleted redox responsive H1299 and HCT116 cells fully restored proliferation to that observed
232 in serine-replete conditions (**Supplementary Figure 4E,G**). In contrast, proliferation of redox
233 unresponsive cells following serine withdrawal had the greatest improvement with simultaneous
234 PHGDH overexpression and FCCP treatment (**Supplementary Figure 4F,G**). This underscores
235 that changes in both the NAD+/NADH ratio and relevant enzyme expression impact serine
236 synthesis in serine depleted environments.

237 To investigate whether FCCP improved serine synthesis and proliferation of redox
238 unresponsive cells through oxidizing the NAD+/NADH ratio, we treated cells with the
239 mitochondrial complex I inhibitor rotenone in conjunction with FCCP. Rotenone treatment blocked
240 the ability of FCCP to improve both proliferation and serine synthesis and suppressed the
241 increase in the NAD+/NADH ratio (**Figure 4H-J, Supplementary Figure 5E,F**). In contrast,
242 treating cells with oligomycin, an ATP synthase inhibitor, did not affect the ability of FCCP to
243 improve proliferation (**Supplementary Figure 4H,I**). This supports the conclusion that FCCP
244 increases serine synthesis and proliferation in serine depleted environments by increasing the
245 NAD+/NADH ratio via mitochondrial complex I-mediated NAD+ regeneration. Moreover, FCCP
246 treatment neither increased PHGDH protein expression nor glucose consumption, indicating that
247 improved proliferation and serine synthesis is not caused by changes in enzyme expression or
248 carbon availability for serine synthesis (**Supplementary Figure 4J,K**). Together, these data
249 argue that mitochondrial respiration, either endogenously increased in response to serine
250 deprivation or as a result of FCCP treatment, can govern the cell NAD+/NADH ratio and directly
251 influence the serine synthesis rate in response to serine withdrawal.

252

253 **The NAD+/NADH ratio influences oxidative citrate synthesis in either serine- or lipid-**
254 **depleted environments**

255 Oxidative biosynthetic reactions other than serine synthesis can be constrained by the
256 NAD+/NADH ratio. For example, cancer cells deprived of environmental lipids increase oxidative
257 citrate production, which can be limited by NAD+ regeneration (Li, 2022) (**Figure 5A,**
258 **Supplementary Figure 6A**). Interestingly, analysis of kinetic U-^{13}C-glucose tracing in cells that
259 showed increased NAD+/NADH ratios following serine deprivation largely showed elevated M+2
260 citrate production despite no change in environmental lipid availability (**Figure 5B;**
261 **Supplementary Figure 6B-E**). In contrast, cells with unaltered NAD+/NADH ratios upon serine
262 depletion did not exhibit higher M+2 citrate production **(Figure 5B; Supplementary Figure 6B,**
263 **F-H)**. Similarly, only cells that increased the NAD+/NADH ratio in response to serine depletion
264 displayed evidence of elevated citrate production from glutamine either through oxidative
265 decarboxylation or reductive carboxylation, both of which require oxidation reactions that can be
266 limited by electron acceptor availability (Hosios and Vander Heiden, 2018; Li, 2022)
267 (**Supplementary Figure 6A, I, J**). To confirm that elevated M+2 citrate synthesis was driven by
268 an increase in the NAD+/NADH ratio, we treated A549 cells depleted of serine with FCCP and
269 examined glucose derived citrate synthesis. Indeed, FCCP treatment led to a four-fold increase
270 in M+2 citrate from U-^{13}C-glucose in A549 cells depleted of serine whereas M+2 citrate synthesis
271 was less affected by FCCP in H1299 cells (**Figure 5C**). The elevated M+2 citrate production in
272 FCCP treated-A549 cells was dependent on mitochondrial complex I, as rotenone prevented the
273 elevated citrate production associated with FCCP treatment (**Supplementary Figure 7A-C**). To
274 confirm that higher M+2 citrate production following FCCP treatment was related to the
275 NAD+/NADH ratio independent of serine deprivation, we treated A549 cells with increasing doses
276 of AKB and FCCP in serine replete conditions and find that increasing the NAD+/NADH ratio with
277 either AKB or FCCP led to elevated M+2 citrate synthesis (**Figure 5D**). This emphasizes that
278 changes to the NAD+/NADH ratio regardless of the nutrient environment can impact citrate
279 synthesis.

280 We next asked whether increasing mitochondrial respiration in response to low
281 extracellular serine was a general response to other nutrient deprivations that increased NAD+
282 demand. To examine this, we depleted A549 and H1299 cells of extracellular lipids by culturing
283 them in media with lipid-depleted serum (Hosios, 2018) and compared oxygen consumption rates
284 to those of cells cultured in media with lipid-containing serum. Surprisingly, we find that A549 cells,
285 which do not increase mitochondrial respiration in response to serine depletion, mildly increase
286 oxygen consumption rates upon lipid depletion. On the other hand, H1299 cells do not increase
287 oxygen consumption in lipid depleted conditions (**Figure 5E**). We next measured the
288 NAD+/NADH ratio of A549 and H1299 cells depleted of environmental lipids. Consistent with the
289 changes in oxygen consumption, A549 cells displayed a slightly increased NAD+/NADH ratio
290 while H1299 cells did not alter the NAD+/NADH ratio upon lipid deprivation (**Figure 5F**).
291 Interestingly, both serine and citrate produced via glucose oxidation were elevated in lipid-
292 deprived A549 cells in comparison to H1299 cells, which exhibited unchanged serine synthesis
293 in response to environmental lipid depletion (**Figure 5G-H, Supplementary Figure 8A-D**). These
294 findings demonstrate that the NAD+/NADH ratio is a determinant of both oxidative citrate and
295 serine synthesis, regardless of environmental demand for the nutrient. Additionally, the different
296 metabolic responses to lipid and serine deprivation between cancer cell types suggests that
297 different nutrient environments may impact mitochondrial respiration through distinct processes
298 to influence the cell NAD+/NADH ratio.
299

300 **Lipid depletion can enhance serine synthesis and proliferation in serine deprived**
301 **conditions**

302 Our finding that both serine and oxidative citrate synthesis are impacted by levels of a
303 different nutrient than that produced by each pathway raised the possibility that the NAD+/NADH
304 ratio coordinates biomass synthesis in response to the availability of multiple oxidized nutrients.
305 Specifically, we hypothesized that changes to the NAD+/NADH ratio caused by one oxidized

306 nutrient depletion could influence the synthesis of, and in turn the dependency on, another
307 oxidized nutrient for proliferation. To begin testing this, we first examined how mitochondrial
308 respiration and the NAD+/NADH ratio were impacted by dual lipid and serine depletion compared
309 to single nutrient depletions in both A549 and H1299 cells. We find that dual depletion of serine
310 and lipids in A549 cells led to elevated oxygen consumption that is comparable to that observed
311 with lipid depletion alone, and higher than that observed with serine depletion alone **(Figure 6A)**.
312 Similarly, dual depletion of serine and lipids in H1299 cells led to elevated oxygen consumption
313 that is comparable to that observed with serine depletion alone, and higher than that observed
314 with lipid depletion alone **(Figure 6A)**. The resulting oxygen consumption rates upon dual serine
315 and lipid starvation corresponded with changes to the cell NAD+/NADH ratio (**Figure 6B**). We
316 then measured the serine and citrate synthesis rates of cells depleted of both extracellular serine
317 and lipids via kinetic U-^{13}C-glucose tracing. Consistent with elevation of the NAD+/NADH ratio
318 after lipid deprivation, A549 cells depleted of both environmental serine and lipids trended towards
319 exhibiting a slightly elevated serine synthesis rate when compared to serine deprivation alone
320 **(Figure 6C).** Moreover, lipid depletion led to a greater fraction of total serine derived from glucose
321 in serine depleted A549 cells **(Supplementary Figure 9A)**. In contrast, lipid starvation did not
322 alter serine synthesis in serine-depleted H1299 cells (**Figure 6D, Supplementary Figure 9B**).
323 Interestingly, in both A549 and H1299 cells, dual serine and lipid deprivation led to elevated citrate
324 production (to a greater degree in H1299 cells) compared to lipid deprivation alone despite only
325 H1299 cells exhibiting a more oxidized NAD+/NADH ratio upon serine depletion (**Figure 6E,F;**
326 **Supplementary Figure 9C,D)**. This underscores the multifactorial regulation of glucose oxidation
327 to citrate (Holness, 2003; Novelli, 1950; Patel, 2006; Srere, 1974). We next asked how cancer
328 cell proliferation was impacted by dual serine and lipid depletion compared to single nutrient
329 depletions. Strikingly, proliferation of serine-depleted A549 cells was improved with depletion of
330 extracellular lipids (**Figure 6G**), consistent with an elevation in mitochondrial respiration,
331 NAD+/NADH ratio, and serine synthesis in A549 cells upon dual serine and lipid depletion. Unlike

332 serine depletion, lipid depletion does not cause a major proliferation defect in either A549 or
333 H1299 cells, and dual serine and lipid deprivation did not greatly alter the proliferation of H1299
334 cells compared to serine depletion alone (**Figure 6H**). This is consistent with lipid deprivation
335 causing no major change in oxygen consumption, NAD+/NADH ratio, and serine synthesis in
336 H1299 cells. Taken together, these data argue that the cell NAD+/NADH ratio is modulated in
337 response to multiple nutrient availabilities in a cancer cell-specific fashion. The changes in
338 NAD+/NADH ratio in turn influence the capacity to synthesize oxidative biomass precursors such
339 as serine and citrate, impacting the proliferation rate of cancer cells in nutrient environments with
340 differing demands for oxidative biomass synthesis.
341

342 **Discussion**

343 Proliferating cancer cells must acquire sufficient biomass and rely on contributions from
344 both environmental biomass precursors and de novo biomass synthesis, but what determines
345 which cells can adapt to different nutrient environments that impose constraints on salvage and
346 de novo synthesis is not known. This study highlights that differential cell responses to change
347 NAD+/NADH ratio enables biomass synthesis and determines whether cells can adapt to
348 proliferate in different nutrient conditions. Importantly, this provides one explanation for why single
349 nutrient levels in tissues may not predict the ability of auxotrophy for a nutrient to determine cancer
350 proliferation in a tissue (Abbott, 2024). It also suggests why cancer proliferation in different
351 nutrient environments is controlled by a complex relationship between cell-intrinsic and cell-
352 extrinsic factors. These factors may be coordinated in part through processes that set the cell
353 NAD+/NADH ratio.

354 Most prior work to determine what shapes the metabolic dependencies of cell proliferation
355 has focused on factors that govern biosynthetic enzyme expression and activity. For example,
356 genomic and transcriptional analyses of cancer discovered that increased PHGDH expression
357 promotes tumor growth (DeNicola, 2015; Locasale, 2011; Newman, 2017; Possemato, 2011) and

358 provides a proliferative advantage in serine depleted tumor microenvironments (Ngo, 2020;
359 Sullivan, 2019b). Our findings show that enzyme expression alone cannot fully explain nutrient
360 dependencies, as PHGDH expression can be discordant with sensitivity to serine depletion.
361 Rather both the NAD+/NADH ratio and enzyme expression play integral roles in determining
362 cancer proliferation in specific nutrient environments. These data are consistent with biosynthetic
363 gene expression and single nutrient levels being unable to predict the tumor tissue environments
364 where cancer cells can form metastases (Abbott, 2024).

365 Extensive work has highlighted the importance of cell NAD+/NADH ratio in influencing
366 oxidized biomass production, nutrient utilization, and nutrient dependencies (Baksh, 2020; Bao,
367 2016; Birsoy, 2015; Broeks, 2023; Christensen, 2014; Diehl, 2019; Garcia-Bermudez, 2018;
368 Gibson, 1976; Krall, 2021; Li, 2022; Schwörer, 2020; Sullivan, 2015; Wu, 2024). Yet, the
369 processes that govern the endogenous NAD+/NADH ratio upon shifts in nutrient availability have
370 been largely uncharacterized. We find that regulation of mitochondrial respiration is a major
371 mechanism that dictates the NAD+/NADH ratio in response to environmental nutrient fluctuations.
372 The mitochondrial respiration response to withdrawal of specific nutrients appears to vary across
373 different cancers. Some cancer cells increased mitochondrial respiration to serine depletion, while
374 others had minimal responses. On the other hand, lipid depletion yielded mitochondrial respiration
375 changes in a different set of cells. No clear common genetic factor or tissue-of-origin was found
376 to align with those cells that do or do not have mitochondrial and redox responses to serine and/or
377 lipid depletion, and further work is needed to understand the mechanisms that enable increased
378 mitochondrial respiration to respond to nutrient deprivation. One possibility is that differences in
379 ATP consumption in response to nutrient deprivation contribute to the response. Stimulating ATP
380 consumption can increase mitochondrial respiration and the NAD+/NADH ratio by modulating
381 mitochondrial membrane potential (Bertholet, 2019; Buttgereit, 1995; Fisher-Wellman, 2012;
382 Luengo, 2021; Nobes, 1989; Vander Heiden, 1999). This suggests that ATP synthase activity can
383 constrain complex I activity to different extents across cancers, modulating the NAD+/NADH ratio

384 and sensitivity to serine or lipid depletion. However, the regulation of complex I, ATP synthesis,
385 and mitochondrial coupling efficiency is complicated and incompletely understood (Alavian, 2014;
386 Gao, 2018; Lapuente-Brun, 2013; Luengo, 2021; Qiu, 2014; Wang, 2022; Yao, 2019; Zhao, 2019).
387 Nevertheless, our findings underscore a relationship between environmental nutrient levels and
388 mitochondrial respiration to influence the NAD+/NADH ratio in cells.

389 Efforts to understand the processes that shape cancer cell metabolic dependencies have
390 largely focused on how cancer cells respond to single nutrient changes. However, through dual
391 serine and lipid depletion experiments, these findings suggest that single nutrient availabilities will
392 be unable to explain cancer metabolic dependencies in some contexts. For example, depleting
393 A549 cells of both extracellular serine and lipids paradoxically improved proliferation relative to
394 serine deprivation alone because the cell NAD+/NADH ratio responds to lipid deprivation to
395 enable increased serine synthesis. This suggests that the NAD+/NADH ratio can serve as a
396 metabolic regulatory node that orchestrates biomass synthesis and integrates changes to multiple
397 oxidized biomass components in the environment, providing a framework for understanding why
398 cancer nutrient dependencies vary across tissue microenvironments (Abbott, 2024). Because
399 oxidizing the cell redox state can increase flux through multiple pathways, the impact of cell redox
400 state on biosynthesis may also explain why some cells lose enzyme expression as this could
401 redirect limited resources toward biomass components that can otherwise be scavenged from the
402 environment (Delage, 2010; Pavlova, 2017; Rabinovich, 2015). Better understanding the
403 mechanisms cells use to alter respiration to adjust the NAD+/NADH ratio in response to nutrient
404 changes could lead to better understanding of the complex interplay between cell-intrinsic and
405 cell-extrinsic factors that determine cancer metabolic dependencies and enable better selection
406 of patients who will respond to therapies targeting metabolism.

407

408 **Materials and Methods**

409 **Cell Culture Experiments**

410 Cell lines were maintained in Dulbecco's Modified Eagle's Medium (DMEM) without sodium
411 pyruvate (Corning 50-013-PC) supplemented with sodium bicarbonate (Sigma S6014) and 10%
412 heat-inactivated Fetal Bovine Serum (FBS). All cells were cultured at 37°C with 5% CO_2, tested
413 for mycoplasma contamination regularly, and confirmed negative before experimentation. Cell
414 line information is listed in Supplementary Table 1.
415
416 **Proliferation Assays**
417 Cells were plated in six-well plates in 2 ml of DMEM with 10% heat-inactivated FBS at an initial
418 seeding density of 40,000 cells. Cells were permitted to settle overnight and then quantified using
419 a sulforhodamine B (SRB) (Sigma Aldrich 230162) colorimetric assay to measure the cell
420 absorbance at the start of the experiment as previously described (Vichai, 2006). For treatment
421 conditions, cells were washed three times with 1 ml of 1X PBS, and 2 ml of treatment media were
422 added to each well. All treatment media was made with 10% dialyzed FBS. Serine-free medium
423 was made by adding a mix of amino acids (Sigma Aldrich) at DMEM concentrations lacking serine
424 and glycine to DMEM with low glucose, without sodium pyruvate, and no amino acids (US
425 Biological D9800-13-50L). Glucose and glycine were supplemented for a final concentration of 25
426 mM and 0.4 mM, respectively. 72 hours after the initial treatment, cells were quantified using SRB
427 assay. All SRB measurements are normalized to a blank to correct for background signal.
428 Proliferation rates were calculated with the following formula:

429 $$\text{Doublings per day} = \frac{\log_2(\text{final SRB absorbance} / \text{SRB absorbance day 0})}{(\text{total \# of treatment days})}$$

430
431
432 **NAD+/NADH Measurements**
433 NAD+/NADH measurements were performed using the NAD/NADH-Glo Assay (Promega G9072)
434 with a modified version of manufacturer instructions as previously reported (Sullivan, 2015). Cells
435 were plated at an initial seeding density of 20,000 cells (A549, H1299, HCT116) or 40,000 cells

436 (Calu6, MDA-MB-231). Cells were permitted to settle overnight. The next day, cells were washed
437 once with 1X PBS and then incubated with 2 ml of treatment media for the indicated times prior
438 to preparation of cell extracts. For extraction, cells were washed once in ice cold 1X PBS and
439 extracted in 100 µl ice-cold 1% dodecyltrimethylammonium bromide (DTAB) in 0.2 N NaOH
440 diluted 1:1 with 1X PBS. Each sample was flash-frozen in liquid nitrogen and immediately stored
441 at -80°C. To measure NADH, 10 µl of sample was moved to PCR tubes, diluted with 10 µl of
442 DTAB, and incubated at 75 °C for 30 min, where basic conditions selectively degrade NAD+. To
443 measure NAD+, 10 µl of the samples was moved to PCR tubes containing 30 µl DTAB and 20 µl
444 0.4 N HCl and incubated at 60°C for 15 min, where acidic conditions selectively degrade NADH.
445 Samples were then allowed to equilibrate to room temperature and quenched by neutralizing with
446 20 µl 0.25 M Tris in 0.2 N HCl (for NADH) or 20 µl 0.5 M Tris base (for NAD+). Manufacturer
447 instructions were followed thereafter to measure NAD+/NADH using a luminometer (Tecan Infinite
448 M200Pro). A standard curve with representative samples was done with each assay to confirm
449 that NAD+ and NADH measurements were in the linear range of detection.

450 **Glucose Consumption and Lactate Secretion Measurements**

451 Cells were plated at a density of 40,000 cells per well in a six well plate. The next day, cells were
452 washed three times with 1X PBS before 2 ml of treatment media were added to each well. In
453 parallel, 2 ml of treatment media were added to plates without cells. An initial cell number before
454 beginning treatment was quantified via Cellometer (Nexcelom Bioscience). 72 hours later, media
455 was collected from exponentially proliferating cells with a parallel collection of media from wells
456 without cells, which we used to measure initial media concentrations to take into consideration
457 evaporative changes. Cell number was quantified via Cellometer along with the volume of media
458 on cells to consider evaporative changes to metabolite concentrations that may have occurred
459 over 72 hours in culture. Glucose concentrations from media samples were measured on a YSI-
460 2900 Biochemistry Analyzer (Yellow Spring Instruments). Every assay included a glucose (Sigma

461 Aldrich G8270) standard curve (0, 2.5, 5, 10, 20, and 40 mM glucose) and lactate (Sigma Aldrich
462 71716) standard curve (0, 1.25, 2.5, 5, 10, and 20 mM sodium lactate), made in both control and
463 treatment media. To calculate consumption rate per cell for a given nutrient, fmol of glucose or
464 lactate over time were plotted relative to the area under the curve (fmol / cells · time) of an
465 exponential function fit to the number of cells at the start of the assay and after 72 hours of
466 treatment, as previously described (Hosios, 2016).
467
468 **Oxygen Consumption Measurements**
469 An Agilent Seahorse Bioscience Extracellular Flux Analyzer (XFe96) was used to measure
470 oxygen consumption rates (OCR). Cells were plated at 20,000 – 40,000 cells per well in a
471 Seahorse Bioscience 96-well plate in 80 µl of DMEM without pyruvate supplemented with 10%
472 heat-inactivated FBS. Cells were not plated on the perimeter of the plate to avoid edge effect.
473 The following day, cells were washed twice with 180 µl of treatment media supplemented with 10%
474 dialyzed FBS before incubating cells with 180 µl of treatment media for the indicated time prior to
475 OCR data acquisition. For 24 hour treatment periods, treatment media was replaced with 180 µl
476 of fresh treatment media two hours before OCR data acquisition. The day before OCR data
477 acquisition, the XFe96 cartridge was hydrated by submerging the sensor cartridge in 200 µl of
478 sterile water per well of the utility plate. Parafilm was wrapped around the perimeter of the
479 cartridge to avoid evaporation. The XFe96 cartridge was then incubated in a 37°C non-CO_2
480 incubator overnight. The next day, at least two hours before data acquisition, the water in the
481 utility plate was replaced with 200 µl of the Agilent XF Calibrant per well and the sensory cartridge
482 was submerged and returned to the 37°C non-CO_2 incubator until OCR was ready to be measured.
483 After OCR data acquisition, six to eight wells per treatment condition were collected for cell
484 number quantification (Cellometer) to normalize OCR values. Basal OCR was calculated by
485 subtracting residual OCR, the OCR remaining following the addition of rotenone and antimycin A
486 for a final concentration of 2 µM each.

487

488 **Kinetic U-^{13}C-Glucose Isotope Tracing Experiments**

489 Cells were seeded at 150,000 cells per well in a six-well plate in 2 ml of DMEM without sodium
490 pyruvate supplemented with 10% heat-inactivated FBS. The following day, cells were washed
491 once with 1 ml of 1X PBS and then incubated in 2 ml of treatment media supplemented with 10%
492 dialyzed FBS for the indicated treatment time and when metabolic steady state is reached. Two
493 hours before the start of the kinetic isotope tracing, media on cells was exchanged with fresh
494 treatment media with 10 mM unlabeled glucose. To measure serine labeling over time in serine-
495 depleted conditions, cells and media were extracted together. Before the initiation of the kinetic
496 U-^{13}C-glucose isotope tracing, serine-depleted cells were washed three times with 1X PBS and
497 then cultured with 400 µl of tracing medium containing 10 mM of U-^{13}C-glucose (Cambridge
498 Isotope Laboratories, CLM-481-0) for the rapid time points. Tracing media was equivalent to
499 treatment media except with 10 mM of U-^{13}C- glucose. Following incubation, 1.6 ml of extraction
500 buffer containing ice cold 100% HPLC-grade methanol (Sigma Aldrich, 646377) with norvaline
501 (Sigma, N7627) was added onto cells with tracing media for a final sample volume of 2 ml (80%
502 extraction buffer and 20% tracing media) and a final concentration of 1 µg per 400 µl norvaline.
503 1.6 ml of the lysate was placed into a fresh Eppendorf tube, vortexed at 4°C at maximum speed
504 for ten minutes, and then spun down at 4°C at maximum speed for thirty minutes. The supernatant
505 was collected and dried under nitrogen gas to prepare for metabolic analysis. To measure serine
506 and citrate production in serine replete conditions, only intracellular metabolites were quantified.
507 Before the initiation of kinetic U-^{13}C-glucose isotope tracing, serine-replete cells were washed
508 three times with 1X PBS and then cultured with 1 ml of tracing medium containing 10 mM of U-
509 ^{13}C-glucose (Cambridge Isotope Laboratories, CLM-481-0) for the rapid time points. Tracing
510 media was equivalent to treatment media except with 10 mM of U-^{13}C- glucose. Following
511 incubation, cells were rapidly washed twice with ice cold blood bank saline. To extract, 500 µl of
512 extraction buffer containing 80% ice cold HPLC-grade methanol and 20% LC-grade water spiked

513 with 1 µg per 400 µl norvaline were added onto cells. Cells were then lysed as previously
514 described above.
515
516 **Gas Chromatography-Mass Spectrometry (GC-MS) Polar Metabolite Measurements**
517 Dried samples were derivatized by adding 16 µl of methoxamine reagent (Thermo Fisher, TS-
518 45950) and incubated for an hour at 37°C followed by the addition of 20 µl of *N-tert-*
519 butyldimethylsilyl-*N*-methyltrifluoroacetamide with 1% *tert*-butyldimethylchlorosilane (Sigma
520 375934). Samples were then incubated for two hours at 60°C. Afterwards, samples were
521 centrifuged at maximum speed for ten minutes, and 20 µl of supernatant was used for analysis.
522 Following derivatization, samples were analyzed using a DB-35MS column (30 m × 0.25 mm
523 i.d. × 0.25 µm, Agilent J&W Scientific) in an Agilent 7890 gas chromatograph coupled to an Agilent
524 5975C mass spectrometer (GC–MS). All ion counts were normalized to internal standard
525 norvaline and cell number measured via Cellometer.
526
527 **Immunoblotting**
528 Cells were washed with ice cold 1X PBS and lysed in cold RIPA buffer containing Halt Protease
529 and Phosphatase Inhibitor Cocktail (Thermo Scientific 78442). Lysates were clarified by rocking
530 samples for thirty minutes at 4°C and then spun at maximum speed for ten minutes for collection
531 of supernatant. Protein concentration was calculating using the BCA Protein Assay (Pierce, 23225)
532 with BSA as a standard. Lysates were resolved by SDS-PAGE using NuPAGE 4-12% Bis-Tris
533 Protein Gels and run at 100 V. Proteins were transferred onto nitrocellulose membranes via wet
534 transfer at 100 V. Membranes were blocked in 5% BSA in 1x TBST before incubating membranes
535 with primary antibodies at 4°C overnight. The next day, membranes were washed three times
536 with 1x TBST at room temperature and then incubated in secondary antibodies for one hour at
537 room temperature. The primary antibodies used were PHGDH (Sigma Aldrich, HPA021241
538 [1:1000]), HSP90 (Cell Signaling Technology, 4874 [1:1000]), and Vinculin (E1E9V) XP® (Cell

539 Signaling Technology, 13901 [1:1000]). The secondary antibodies used were anti-rabbit IgG
540 horseradish peroxidase-linked antibody (1:4000 dilution; Cell Signaling Technologies, 7074S) or
541 anti-mouse IgG horseradish peroxidase-linked antibody (1:4000, 7076S).
542
543 **Cell Line Generation**
544 Cell lines overexpressing either EGFP or human PHGDH were generated via lentiviral infection.
545 pLJM1-EGFP was obtained from Addgene (Addgene plasmid # 19319). pLJM1-PHGDH was
546 constructed using pLJM1-Empty (Addgene plasmid # 91980) as a backbone. pLJM1-Empty was
547 digested using NheI and EcoRI and gel purified. Human PHGDH cDNA was amplified from
548 pLHCX-PHGDH (PMID: 31598584) with the following oligonucleotide primers, where the
549 capitalized sequence denotes PHGDH homology:
550 PHGDH F: agtgaaccgtcagatccggctagcgccaccATGGCTTTTGCAAATCTGCG
551 PHGDH R: tactgccatttgtctcgaggtcgagaattcTTAGAAGTGGAACTGGAAGGCT
552 PHGDH insert was gradient PCR amplified using Phusion High-Fidelity DNA polymerase (NEB
553 M0530) from 60 to 70°C and gel purified. Digested pLJM1-Empty and amplified PHGDH insert
554 were assembled via Gibson Assembly, and the resulting plasmid was transformed, and
555 validated by Sanger sequencing. Lentiviral production was done by transfecting constructs into
556 LentiX293T cells with Mirus Transit293T (Mirus Bio MIR2700) following manufacturer's protocol.
557 Briefly, 800,000 cells were plated per well in a 6 well plate in DMEM media with 10% heat-
558 inactivated FBS. The next day, cells were transfected with 1.6 µg vector (either pLJM1-EGFP or
559 pLJM1-PHGDH), 800 ng of pMDLg (Addgene plasmid # 12251) packaging plasmid, 400 ng of
560 pMD2.G (Addgene plasmid # 12259) envelope plasmid, and 400 ng of pRSV-REV (Addgene
561 plasmid # 12253) in OptiMEM (Thermo Fisher Scientific 31985070). DNA transfection mix was
562 incubated with cells for 48 hours before harvesting virus and filtering through a 0.45 µm
563 polyethersulfone membrane. Sub-confluent cells were infected with 1 ml of virus-containing
564 media in each well of a 6 well plate with polybrene (8 µg/ml, EMD Millipore TR-1003-G). 24

565 hours after infection, selection with 1 μg/mL puromycin (Sigma Aldrich P7255) began. All
566 experiments with generated cell lines were conducted on a polyclonal cell population.
567
568 **Statistics and Reproducibility**
569 All statistical tests using experimental data were performed with Prism 10 software. No statistical
570 method was used to predetermine sample sizes. Samples sizes were chosen based on pilot
571 experiments using three or more technical replicates. Certain data points were excluded from
572 Seahorse analyzer assays due to premature injection of rotenone and antimycin. The experiments
573 were not randomized and the investigators were not blinded during experiments nor data analysis.
574
575 **Acknowledgements**
576 We thank all members of the Vander Heiden lab for helpful discussions, Emma Dawson, Grace
577 Wolczanski, and Alejandra Rosario-Crespo for technical assistance, and Jessica Spinelli for
578 assistance with using Seahorse equipment during the COVID-19 pandemic. The authors
579 acknowledge support from F30CA268633 (SMC), T32GM007287 (SMC, MBM, ASZ, KLA), the
580 Kosciuszko Foundation (SET), NSF DGE-1122374 (KLA), and F31CA271787 (KLA), as well as
581 support to MGVH from the Ludwig Center at MIT, the MIT Center for Precision Cancer Medicine,
582 and the NCI (R35CA242379, R01CA259253, P30CA1405141).
583
584 **Author Contributions**
585 Conceptualization: SMC, MGVH; Intellectual Discussion: SMC, MBM, MGVH; Proliferation rates:
586 SMC, SET, ASZ; Kinetic Isotope Tracing: SMC, SET, MBM; Immunoblotting: SMC, SET;
587 NAD+/NADH measurements: SMC, SET; Oxygen consumption: SMC; Overexpression constructs:
588 KLA; Cell line generation: SMC; Writing: SMC and MGVH; Editing: SMC, MBM, SET, ASZ, KLA,
589 MGVH; Funding Acquisition: MGVH
590

591 **Competing Interests**

592 M.G.V.H. discloses that he is a scientific advisor for Agios Pharmaceuticals, iTeos Therapeutics,
593 Sage Therapeutics, Pretzel Therapeutics, Lime Therapeutics, Faeth Therapeutics, Droia
594 Ventures, MPM Capital and Auron Therapeutics. All remaining authors declare no competing
595 interests.

596

597 **References**

598 Abbott, K.L., Subudhi, S., Ferreira, R., Gültekin, Y., Steinbuch, S.C., Bin Munim, M., Honeder,
599 S.E., Kumar, A.S., Ramesh, D.L., Wu, M., Hansen, J.A., Sivanand, S., Reidmayr, L.M.,
600 Duquette, M., Ali, A., Henning, N., Shevzov-Zebrun, A., Gourgue, F., Barbeau, A.M., Waite, M.,
601 Kunchok, T., Ferraro, G.B., Do, B.T., Spanoudaki, V., Sánchez-Rivera, F.J., Jin, X., Church,
602 G.M., Jain, R.K., Vander Heiden, M.G. (2024). Site of breast cancer metastasis is independent
603 of single nutrient levels. bioRxiv. 10.1101/2024.10.24.616714.
604
605 Alavian, K.N., Beutner, G., Lazrove, E., Sacchetti, S., Park, H.-A., Licznerski, P., Li, H., Nabili,
606 P., Hockensmith, K., Graham, M., Porter, G. A., & Jonas, E. A. (2014). An uncoupling channel
607 within the c-subunit ring of the F1FO ATP synthase is the mitochondrial permeability transition
608 pore. PNAS *111*, 10580–10585. https://doi.org/10.1073/pnas.1401591111.
609
610 Apiz Saab, J.J., Dzierozynski, L.N., Jonker, P.B., AminiTabrizi, R., Shah, H., Elena Menjivar, R.,
611 Scott, A.J., Nwosu, Z.C., Zhu, Z., Chen, R.N., Oh, M., Sheehan, C., Wahl, D.R., Rasca di
612 Magliano, M., Lyssiotis, C.A., Macleod, K.F., Weber, C.R., Muir, A. (2023). Pancreatic tumors
613 exhibit myeloid-driven amino acid stress and upregulate arginine biosynthesis. eLife *12*.
614 https://doi.org/10.7554/eLife.81289.
615
616 Baksh, S.C., Todorova, P.K., Gur-Cohen, S., Hurwitz, B., Ge, Y., Novak, J.S.S., Tierney, M.T.,
617 dela Cruz-Racelis, J., Fuchs, E., Finley, L.W.S. (2020). Extracellular serine controls epidermal
618 stem cell fate and tumour initiation. Nature Cell Biology *22*, 779-790.
619 https://doi.org/10.1038/s41556-020-0525-9.
620
621 Banh, R.S., Biancur, D.E., Yamamoto, K., Sohn, A.S.W., Walters, B., Kuljanin, M., Gikandi, A.,
622 Wang, H., Mancias, J.D., Schneider, R.J., Pacold, M.E., Kimmelman, A.C. (2020). Neurons
623 Release Serine to Support mRNA Translation in Pancreatic Cancer. Cell *183*, 1202-1218.
624 10.1016/j.cell.2020.10.016.
625
626 Bao, X.R., Ong, S.-E., Goldberger, O., Peng, J., Sharma, R., Thompson, D. A., Vafai, S. B.,
627 Cox, A. G., Marutani, E., Ichinose, F., Goessling, W., Regev, A., Carr, S. A., Clish, C. B., &
628 Mootha, V. K. (2016). Mitochondrial dysfunction remodels one-carbon metabolism in human
629 cells. eLife *5*. https://doi.org/10.7554/elife.10575.
630
631 Bertholet, A.M., Chouchani, E. T., Kazak, L., Angelin, A., Fedorenko, A., Long, J. Z., Vidoni, S.,
632 Garrity, R., Cho, J., Terada, N., Wallace, D. C., Spiegelman, B. M., & Kirichok, Y. (2019). H+
633 transport is an integral function of the mitochondrial ADP/ATP carrier. Nature *571*, 515–520.
634 https://doi.org/10.1038/s41586-019-1400-3.

Birsoy, K., Wang, T., Chen, W.W., Freinkman, E., Abu-Remaileh, M., Sabatini, D.M. (2015). An Essential Role of the Mitochondrial Electron Transport Chain in Cell Proliferation Is to Enable Aspartate Synthesis. Cell *162*, 540-551. https://doi.org/10.1016/j.cell.2015.07.016.

Broeks, M.H., Meijer, N.W.F., Westland, D., Bosma, M., Gerrits, J., German, H.M., Ciapaite, J., van Karnebeek, C.D.M., Wanders, R.J.A., Zwartkruis, F.J.T., Verhoeven-Duif, N., Jans, J.J.M. (2023). The malate-aspartate shuttle is important for de novo serine biosynthesis. Cell Reports *42*. https://doi.org/10.1016/j.celrep.2023.113043.

Buttgereit, F., Brand, M.D. (1995). A hierarchy of ATP-consuming processes in mammalian cells. Biochemical Journal *312*, 163-167. A hierarchy of ATP-consuming processes in mammalian cells.

Chang, S.M. (2024). Control of Cellular Redox State and Biomass Synthesis. PhD Thesis *Massachusetts Institute of Technology* https://dspace.mit.edu/handle/1721.1/155353.

Christensen, C.E., Karlsson, M., Winther, J.R., Jensen, P.R., Lerche, M.H. (2014). Non-invasive In-cell Determination of Free Cytosolic [NAD+]/[NADH] Ratios Using Hyperpolarized Glucose Show Large Variations in Metabolic Phenotypes. Journal of Biological Chemistry *289*, 2344-2352. 10.1074/jbc.M113.498626.

Cognet, G., Muir, A. (2024). Identifying metabolic limitations in the tumor microenvironment. Science Advances *10*. 10.1126/sciadv.adq7305.

Deberardinis, R.J., Lum, J.J., Hatzivassiliou, G., Thompson, C.B. (2008). The Biology of Cancer: Metabolic Reprogramming Fuels Cell Growth and Proliferation. Cell Metabolism *7*, 11-20.

Delage, B., Fennell, D.A., Nicholson, L., McNeish, I., Lemoine, N.R., Crook, T., Szlosarek, P.W. (2010). Arginine deprivation and argininosuccinate synthetase expression in the treatment of cancer. International Journal of Cancer *126*, 2762-2772. 10.1002/ijc.25202.

DeNicola, G.M., Chen P., Mullarky E., Sudderth, J.A., Hu, Z., Wu, D., Tang, H., Xie, Y., Asara J.M., Huffman, K.E., Wistuba, I.I., Minna, J.D., DeBerardinis, R.J., Cantley, L.C. (2015). NFR2 regulates serine biosynthesis in non-small cell lung cancer. Nature Genetics *47*, 1475-1481. 10.1038/ng.3421.

Diehl, F.F., Lewis, C.A., Fiske, B.P., Vander Heiden, M.G. (2019). Cellular redox state constrains serine synthesis and nucleotide production to impact cell proliferation. Nature Metabolism *1*, 861-867. doi:10.1038/s42255-019-0108-x.

Fantin, V.R., St-Pierre, J., Leder, P. (2006). Attenuation of LDH-A expression uncovers a link between glycolysis, mitochondrial physiology, and tumor maintenance. Cancer Cell *9*, 425-434. 10.1016/j.ccr.2006.04.023.

Faubert, B., Solmonson, A., Deberardinis, R.J. (2020). Metabolic reprogramming and cancer progression. Science *368*. DOI: 10.1126/science.aaw5473.

Ferraro, G.B., Ali, A., Luengo, A., Kodack, D.P., Deik, A., Abbott, K.L., Bezwada, D., Blanc, L., Prideaux, B., Jin, X., Possada, J.M., Chen, J., Chin, C.R., Amoozgar, Z., Ferreira, R., Chen, I.,

686 Naxerova, K., Ng, C., Westermark, A.M., Duquette, M., Roberge, S., Lindeman, N.I., Lyssiotis,
687 C.A., Nielsen, J., Housman, D.E., Duda, D.G., Brachtel, E., Golub, T.R., Cantley, L.C., Asara,
688 J.M., Davidson, S.M., Fukumua, D., Dartois, V.A., Clish, C.B., Jain, R.K., Vander Heiden, M.G.
689 (2021). Fatty acid synthesis is required for breast cancer brain metastasis. Nature Cancer *2*,
690 414-428. https://doi.org/10.1038/s43018-021-00183-y.
691
692 Fisher-Wellman, K.H., Neufer, P.D. (2012). Linking mitochondrial bioenergetics to insulin
693 resistance via redox biology. Trends in Endocrinology & Metabolism *23*, 142-153.
694 10.1016/j.tem.2011.12.008.
695
696 Gao, X., Lee, K., Reid, M.A., Sanderson, S.M., Qiu, C., Li, S., Liu, J., Locasale, J.W. (2018).
697 Serine Availability Influences Mitochondrial Dynamics and Function through Lipid Metabolism.
698 Cell Reports *22*, 3507-3520. https://doi.org/10.1016/j.celrep.2018.03.017.
699
700 Garcia-Bermudez, J., Baudrier, L., La, K., Ge Zhu, X., Fidelin, J., Sviderskiy, V.O.,
701 Papagiannakopoulos, T., Molina, H., Snuderl, M., Lewis, C.A., Possemato, R.L., Birsoy, K.
702 (2018). Aspartate is a limiting metabolite for cancer cell proliferation under hypoxia and in
703 tumours. Nature Cell Biology *20*, 775-781. 10.1038/s41556-018-0118-z.
704
705 Gibson, G., Blass, J.P. (1976). A Relation between [NAD+]/[NADH] Potentials and Glucose
706 Utilization in Rat Brain Slices. Journal of Biological Chemistry *251* (*13*), 4127-4130.
707
708 Gravel, S., Hulea, L., Toban, N., Birman, E., Blouin, M., Zakikhani, M., Zhao, Y., Topisirovic, I.,
709 St-Pierre, J., Pollak, M. (2014). Serine Deprivation Enhances Antineoplastic Activity of
710 Biguanides. Cancer Research *74*, 7521-7533. https://doi.org/10.1158/0008-5472.CAN-14-2643-
711 T.
712
713 Gullino, P.M., Clark, S.H., Grantham, F.H. (1964). The Interstitial Fluid of Solid Tumors. Cancer
714 Research *24*, 780-797.
715
716 Hanahan, D., Weinberg, R.A. (2011). Hallmarks of Cancer: The Next Generation. Cell *144*,
717 646–674. https://doi.org/10.1016/j.cell.2011.02.013.
718
719 Handy, D.E., Loscalzo, J. (2012). Redox Regulation of Mitochondrial Function. Antioxidants &
720 Redox Signaling *16*, 1323-1367. 10.1089/ars.2011.4123.
721
722 Holness, M.J., Sugden, M.C. (2003). Regulation of pyruvate dehydrogenase complex activity by
723 reversible phosphorylation. Biochemical Society Transactions *31* (*6*), 1143-1151.
724 10.1042/bst0311143.
725
726 Hosios, A.M., Hecht, V.C., Danai, L.V., Johnson, M.O., Rathmell, J.C., Steinhauser, M.L.,
727 Manalis, S.R., Vander Heiden, M.G. (2016). Amino acids rather than glucose account for the
728 majority of cell mass in proliferating mammalian cells. Developmental Cell *36*, 540-549. doi:
729 10.1016/j.devcel.2016.02.012.
730
731 Hosios, A.M., Li, Z., Lien, E.C., Vander Heiden, M.G. (2018). Preparation of Lipid-Stripped
732 Serum for the Study of Lipid Metabolism in Cell Culture. Bio-protocol *8*.
733 10.21769/BioProtoc.2876
734

735 Hosios, A.M., and Vander Heiden, M.G. (2018). The redox requirement of proliferation
736 mammalian cells. Journal of Biological Chemistry *293*, 7490-7498.
737 https://doi.org/10.1074/jbc.TM117.000239.
738
739 Krall, A.S., Mullen, P.J., Surjano, F., Momcilovic, M., Schmid, E.W., Halbrook, C.J., Thambundit,
740 A., Mittelman, S.D., Lyssiotis, C.A., Shackelford, D.B., Knott, S.R.V., Christofk, H.R. (2021).
741 Asparagine couples mitochondrial respiration to ATF4 activity and tumor growth. Cell
742 Metabolism *33*, 1013-1026. https://doi.org/10.1016/j.cmet.2021.02.001.
743
744 Labuschagne, C.F., van den Broek, N.J.F., Mackay, G.M., Vousden, K.H., Maddocks, O.D.K.
745 (2014). Serine, but not glycine, supports one-carbon metabolism and proliferation of cancer
746 cells. Cell Reports *7*. doi: 10.1016/j.celrep.2014.04.045.
747
748 Lapuente-Brun, E., Moreno-Loshuertos, R., Acin-Perez, R., Latorre-Pellicer, A., Colas, C.,
749 Balsa, E., Perales-Clemente, E., Quiros, P.M., Calvo, E., Rodriguez-Hernandez, M.A., Navas,
750 P., Cruz, R., Carracedo, A., Lopez-Otin, C., Perez-Martos, A., Fernandez-Silva, P., Fernandez-
751 Vizarra, E., Enriquez, J.A. (2013). Supercomplex Assembly Determines Electron Flux in the
752 Mitochondrial Electron Transport Chain. Science *340*, 1567-1570. 10.1126/science.1230381.
753
754 Li, Z., Ji, B.W., Dixit, P.D., Lien, E.C., Tchourine, K., Hosios, A.M., Abbott, K.L., Westermark,
755 A.M., Gorodetsky, E.F., Sullivan, L.B., Vander Heiden, M.G., Vitkup, D. (2022). Cancer cells
756 depend on environmental lipids for proliferation when electron acceptors are limited. Nature
757 Metabolism *4*, 711-723. https://doi.org/10.1038/s42255-022-00588-8.
758
759 Locasale, J.W., Grassian, A.R., Melman, T., Lyssiotis, C.A., Mattaini, K.R., Bass, A.J., Heffron,
760 G., Metallo, C.M., Muranen, T., Sharfi, H., Sasaki, A.T., Anastasiou, D., Mullarky, E., Vokes,
761 N.I., Sasaki, M., Beroukhim, R., Stephanopoulos, G., Ligon, A.H., Meyerson, M., Richardson,
762 A.L., Chin, L., Wagner, G., Asara, J.M., Brugge, J.S., Cantley, L.C., Vander Heiden, M.G.
763 (2011). Phosphoglycerate dehydrogenase diverts glycolytic flux and contributes to oncogenesis.
764 Nature Genetics *43*, 869-874. 10.1038/ng.890.
765
766 Luengo, A., Li, Z., Gui, D. Y., Sullivan, L. B., Zagorulya, M., Do, B. T., Ferreira, R., Naamati, A.,
767 Ali, A., Lewis, C. A., Thomas, C. J., Spranger, S., Matheson, N. J., & Vander Heiden, M. G.
768 (2021). Increased demand for NAD+ relative to ATP drives aerobic glycolysis. Molecular Cell
769 *81*, 691–707. https://doi.org/10.1016/j.molcel.2020.12.012.
770
771 Lyssiotis, C.A., Kimmelman, A.C. (2017). Metabolic Interactions in the Tumor Microenvironment.
772 Trends in Cell Biology *27*, 863-875. https://doi.org/10.1016/j.tcb.2017.06.003.
773
774 Maddocks, O.D.K., Athineos, D., Cheung, E. C., Lee, P., Zhang, T., Van Den Broek, N. J. F.,
775 Mackay, G. M., Labuschagne, C. F., Gay, D., Kruiswijk, F., Blagih, J., Vincent, D. F., Campbell,
776 K. J., Ceteci, F., Sansom, O. J., Blyth, K., & Vousden, K. H. (2017). Modulating the therapeutic
777 response of tumours to dietary serine and glycine starvation. Nature *544*, 372–376.
778 https://doi.org/10.1038/nature22056.
779
780 Maddocks, O.D.K., Berkers, C. R., Mason, S. M., Zheng, L., Blyth, K., Gottlieb, E., & Vousden,
781 K. H. (2013). Serine starvation induces stress and p53-dependent metabolic remodelling in
782 cancer cells. Nature *493* (*7433*), 542–546. https://doi.org/10.1038/nature11743.
783
784 McLaughlin, S.G., Dilger, J.P. (1980). Transport of protons across membranes by weak acids.
785 Physiological Reviews *60* (*3*), 825-863. 10.1152/physrev.1980.60.3.825.

786 Newman, A.C., Maddocks, O.D.K. (2017). One-carbon metabolism in cancer. British Journal of
787 Cancer *116*, 1499-1504. https://doi.org/10.1038/bjc.2017.118.
788
789 Ngo, B., Kim, E., Osorio-Vasquez, V., Doll, S., Bustraan, S., Liang, R. J., Luengo, A., Davidson,
790 S. M., Ali, A., Ferraro, G. B., Fischer, G. M., Eskandari, R., Kang, D. S., Ni, J., Plasger, A.,
791 Rajasekhar, V. K., Kastenhuber, E. R., Bacha, S., Sriram, R. K., … Pacold, M. E. (2020).
792 Limited Environmental Serine and Glycine Confer Brain Metastasis Sensitivity to PHGDH
793 Inhibition. Cancer Discovery *10*, 1352–1373. https://doi.org/10.1158/2159-8290.cd-19-1228.
794
795 Nobes, C.D., Lakin-Thomas, P.L., Brand, M.D. (1989). The contribution of ATP turnover by the
796 Na+/K+-ATPase to the rate of respiration of hepatocytes: Effects of thyroid status and fatty
797 acids. Biochimica Et Biophysica Acta (BBA) - Bioenergetics *976*, 241-245.
798 https://doi.org/10.1016/S0005-2728(89)80236-1.
799
800 Novelli, G.D., Lipmann, F. (1950). The Catalytic Function of Coenzyme A in Citric Acid
801 Synthesis. Journal of Biological Chemistry *182*, 213-228.
802
803 Patel, M.S., Korotchkina, L.G. (2006). Regulation of the pyruvate dehydrogenase complex.
804 Biochemical Society Transactions *34* (*2*), 217-222. 10.1042/BST20060217.
805
806 Pavlova, N.N., Thompson, C.B. (2017). The Emerging Hallmarks of Cancer Metabolism. Cell
807 Metabolism *23*, 27-47. 10.1016/j.cmet.2015.12.006.
808
809 Possemato, R., Marks, K.M., Shaul, Y.D., Pacold, M.E., Kim, D., Birsoy, K., Sethumadhavan,
810 S., Woo, H., Jang, H.G., Jha, A.K., Chen, W.W., Barrett, F.G., Stransky, N., Tsun, Z., Cowley,
811 G.S., Barretina, J., Kalaany, N.Y., Hsu, P.P., Ottina, K., Chan, A.M., Yuan, B., Garrayway, L.A.,
812 Root, D.E., Mino-Kenudson, M., Brachtel, E.F., Driggers, E.M., Sabatini, D.M. (2011).
813 Functional genomics reveals serine synthesis is essential in PHGDH-amplified breast cancer.
814 Nature *476*, 346-350. 10.1038/nature10350.
815
816 Qiu, F., Chen, Y.-R., Liu, X., Chu, C.-Y., Shen, L.-J., Xu, J., Gaur, S., Forman, H. J., Zhang, H.,
817 Zheng, S., Yen, Y., Huang, J., Kung, H.-J., & Ann, D. K. (2014). Arginine Starvation Impairs
818 Mitochondrial Respiratory Function in ASS1-Deficient Breast Cancer Cells. Science Signaling *7*,
819 ra31.
820
821 Rabinovich, S., Adler, L., Yizhak, K., Sarver, A., Silberman, A., Agron, S., Stettner, N., Sun, Q.,
822 Brandis, A., Helbling, D., Korman, S., Itzkovitz, S., Dimmock, D., Ulitsky, I., Nagamani, S. C. S.,
823 Ruppin, E., & Erez, A. (2015). Diversion of aspartate in ASS1-deficient tumours fosters de novo
824 pyrimidine synthesis. Nature *527*, 379-383. https://doi.org/10.1038/nature15529.
825
826 Schwörer, S., Berisa, M., Violante, S., Qin, W., Zhu, J., Hendrickson, R.C., Cross, J.R.,
827 Thompson, C.B. (2020). Proline biosynthesis is a vent for TGFβ-induced mitochondrial redox
828 stress. The EMBO Journal *39*. https://doi.org/10.15252/embj.2019103334.
829
830 Sciacovelli, M., Dugourd, A., Valcarcel Jimenez, L., Yang, M., Nikitopoulou, E., Costa, A.S.H.,
831 Tronci, L., Caraffini, V., Rodrigues, P., Schmidt, C., Gerard Ryan, D., Young, T., Zecchini, V.R.,
832 Rossi, S.H., Massie, C., Lohoff, C., Masid, M., Hatzimanikatis, V., Kuppe, C., Kriegsheim, A.V.,
833 Kramann, R., Gnanapragasam, V., Warren, A.Y., Stewart, G.D., Erez, A., Vanharanta, S., Saez-
834 Rodriguez, J., Frezza, C. (2022). Dynamic partitioning of branched-chain amino acids-derived
835 nitrogen supports renal cancer progression. Nature Communications *13* (*7830*).
836 10.1038/s41467-022-35036-4.

Sivanand, S., Gultekin, Y., Winter, P.S., Vermeulen, S.Y., Tchourine, K.M., Abbott, K.L., Danai, L.V., Gourge, F., Do, B.T., Crowder, K., Kunchok, T., Lau, A.N., Darnell, A.M., Jefferson, A., Morita, S., Duda, D.G., Aguirre, A.J., Wolpin, B.M., Henning, N., Spanoudaki, V., Maiorino, L., Irvine, D.J., Yilmaz, O.H., Lewis, C.A., Vitkup, D., Shalek, A.K., Vander Heiden, M.G. (2024). Cancer tissue of origin constrains the growth and metabolism of metastases. Nature Metabolism *6*, 1668-1681. 10.1038/s42255-024-01105-9.

Srere, P.A. (1974). Controls of citrate synthase activity. Life Sciences *15*, 1695-1710.

Sullivan, L.B., Gui, D.Y., Hosios, A.M., Bush, L.N., Freinkman, E., Vander Heiden M.G. (2015). Supporting Aspartate Biosynthesis Is an Essential Function of Respiration in Proliferation Cells. Cell *162*, 552-563. doi:10.1016/j.cell.2015.07.017.

Sullivan, M.R., Danai, L. V., Lewis, C. A., Chan, S. H., Gui, D. Y., Kunchok, T., Dennstedt, E. A., Vander Heiden, M. G., Muir, A. (2019a). Quantification of microenvironmental metabolites in murine cancers reveals determinants of tumor nutrient availability. eLife *8*. https://doi.org/10.7554/elife.44235.

Sullivan, M.R., Mattaini, K.R., Dennstedt, E.A., Nguyen, A.A., Reilly, M.F., Meeth, K., Muir, A., Darnell, A.M., Bosenberg, M.W., Lewis, C.A., Vander Heiden, M.G. (2019b). Increased serine synthesis provides an advantage for tumors arising in tissues where serine levels are limiting. Cell Metabolism *29*, 1410-1421,e1414. doi: 10.1016/j.cmet.2019.02.015.

Terada, H. (1990). Uncouplers of Oxidative Phosphorylation. Environmental Health Perspectives *87*, 213-218. 10.1289/ehp.9087213.

Vander Heiden, M.G., Chandel, N.S., Schumacker, P.T., Thompson, C.B. (1999). Bcl-xL Prevents Cell Death following Growth Factor Withdrawal by Facilitating Mitochondrial ATP/ADP Exchange. Molecular Cell *3*, 159-167. https://doi.org/10.1016/S1097-2765(00)80307-X.

Vander Heiden, M.G., Deberardinis R.J. (2017). Understanding the Intersections between Metabolism and Cancer Biology. Cell *168*, 657-669. doi:10.1016/j.cell.2016.12.039.

Vichai, V., Kirtikara, K. (2006). Sulforhodamine B colorimetric assay for cytotoxicity screening. Nature Protocols *1*, 1112-1116. https://doi-org.ezp-prod1.hul.harvard.edu/10.1038/nprot.2006.179.

Wang, Y., Stancliffe, E., Fowle-Grider, R., Wang, R., Wang, C., Schwaiger-Haber, M., Shriver, L.P., Patti, G.J. (2022). Saturation of the mitochondrial NADH shuttles drives aerobic glycolysis in proliferating cells. Molecular Cell *82*, 3270-3283. https://doi.org/10.1016/j.molcel.2022.07.007.

Wu, Z., Bezwada, D., Cai, F., Harris, R.C., Ko, B., Sondhi, V., Pan, C., Vu, H.S., Nguyen, P.T., Faubert, B., Cai, L., Chen, H., Martin-Sandoval, M., Do, D., Gu, W., Zhang, Y., Zhang, Y., Brooks, B., Kelekar, S., Zacharias, L.G., Oaxaca, K.C., Patricio, J.S., Mathews, T.P., Garcia-Bermudez, J., Ni, M., DeBerardinis, R.J., (2024). Electron transport chain inhibition increases cellular dependence on purine transport and salvage. Cell Metabolism *36*, 1504-1520. https://doi.org/10.1016/j.cmet.2024.05.014.

886 Yao, C., Wang, R., Wang, Y., Kung, C., Weber, J.D., Patti, G.J. (2019). Mitochondrial fusion
887 supports increased oxidative phosphorylation during cell proliferation. eLife *8*.
888 10.7554/eLife.41351.
889
890 Zhao, R., Jiang, S., Zhang, L., Yu, Z. (2019). Mitochondrial electron transport chain, ROS
891 generation, and uncoupling International Journal of Molecular Medicine *44*, 3-15.
892 10.3892/ijmm.2019.4188.
893

894

895 **Figure Legends**

896

897 **Figure 1. The NAD+/NADH ratio is proportional to serine synthesis rate. (A)** α-ketobutyrate
898 (AKB) is an exogenous electron acceptor that promotes the oxidation of NADH into NAD+ through
899 its conversion to α-hydroxybutyrate (AHB). Rotenone inhibits activity of complex I of the
900 mitochondrial electron transport chain (ETC) to block NADH oxidation into NAD+. **(B)**
901 NAD+/NADH ratio measured in A549 cells cultured without serine and indicated concentrations
902 of AKB (left) and rotenone (right) for 24 hours. NAD+/NADH ratios are normalized to untreated
903 cells cultured without serine, n=3. **(C)** Schematic depicting NAD+ requirement to produce serine
904 labeled (M+3) from U-^{13}C-glucose. Under culture conditions without serine, intracellular serine
905 rapidly effluxes from cells into culture media. Thus, cells and media were jointly analyzed at each
906 time point of kinetic tracing to better capture serine levels. **(D)** Serine labeled (M+3) from U-^{13}C-
907 glucose over time in A549 cells cultured without serine and with indicated concentrations of AKB
908 and rotenone for 24 hours prior to U-^{13}C-glucose exposure. Serine levels are normalized to
909 internal norvaline standard and cell number measured in indicated conditions, n=3. **(E)** Relative
910 NAD+/NADH ratios from A549 cells cultured without serine after exposure to 250 μM AKB, 1000
911 μM AKB, 20 nM rotenone, or 40 nM rotenone for 24 hours are plotted against the serine synthesis
912 rates from corresponding conditions as shown in D. Serine synthesis rates are calculated from
913 labeled serine (M+3) after 1 and 15 minutes of U-^{13}C-glucose exposure and normalized to
914 untreated and serine-free culture conditions, n=3. **(F)** Proliferation rate (doublings per day) of

915 A549 cells cultured with and without serine and the indicated concentration of AKB for 72 hours,
916 n=3. **(G)** Proliferation rate (doublings per day) of A549 cells cultured with and without serine and
917 the indicated concentration of rotenone for 72 hours, n=3. Data shown represent means ± SD.
918
919 **Figure 2. The NAD+/NADH ratio differs between cancer cells upon serine withdrawal and**
920 **correlates with proliferation in serine-depleted conditions. (A)** Proliferation rate (doublings
921 per day) of indicated cancer cells cultured without serine for 72 hours normalized to proliferation
922 rate of corresponding cancer cells cultured with serine, n=3. **(B)** NAD+/NADH ratios of indicated
923 cells cultured with and without serine for 24 hours. Yellow indicates cells with unaltered
924 NAD+/NADH ratios and blue indicates cells with elevated NAD+/NADH ratios when cultured
925 without serine. Values are normalized to the NAD+/NADH ratios of cells cultured with serine, n=3.
926 **(C)** Relative NAD+/NADH ratios of cells cultured without serine as shown in B are plotted against
927 proliferation rates of corresponding cells cultured without serine. Data points denote the different
928 cell lines (Calu6, A549, 8988T, MIA PaCa-2, H1299, and HCT116). **(D)** Serine labeled (M+3) from
929 U-^{13}C-glucose over time in A549 and H1299 cells cultured with and without serine for 24 hours
930 prior to U-^{13}C-glucose exposure. Serine levels are normalized to internal norvaline standard and
931 cell number measured in indicated conditions, n=3. **(E)** Absolute fold change of serine labeled
932 (M+3) from U-^{13}C-glucose in A549 and H1299 cells cultured without serine relative to serine
933 labeled (M+3) from U-^{13}C-glucose in A549 and H1299 cells cultured with serine for 24 hours after
934 twelve minutes of U-^{13}C-glucose exposure, n=3. Data shown are means ± SD. P-values were
935 calculated by unpaired Student's t-test, **$p<0.01$, ***$p<0.001$
936
937 **Figure 3. Elevated mitochondrial respiration is associated with increased NAD+/NADH**
938 **ratios and serine synthesis rates. (A)** Oxygen consumption rate (OCR) of indicated cells
939 cultured with and without serine for 24 hours. Values are averages of three repeat measurements,

940 n=14-20. **(B)** OCR of cells (H1299 top, A549 bottom) cultured with indicated concentrations of
941 serine for 24 hours. Values are averages of three repeat measurements, n=3-9. **(C)** NAD+/NADH
942 ratios of cells (H1299 top, A549 bottom) cultured with indicated concentrations of serine for 24
943 hours. Values are normalized to the NAD+/NADH ratio of cells cultured in 400μM serine (serine
944 concentration in DMEM), n=3. **(D)** Relative OCR plotted against NAD+/NADH ratios in H1299 and
945 A549 cells cultured in 0, 25, 50, and 100 μM serine for 24 hours. OCR and NAD+/NADH ratios
946 are normalized to measurements from the 100 μM serine condition, n=3. **(E)** Serine labeled (M+3)
947 from U-^{13}C-glucose over time in cells (H1299 top, A549 bottom) cultured with indicated serine
948 concentrations for 24 hours prior to U-^{13}C-glucose exposure. Serine levels are normalized to
949 internal norvaline standard and cell number measured in indicated conditions, n=3. **(F)** Relative
950 NAD+/NADH ratios of cells (H1299 top, A549 bottom) cultured with 0, 25, 50, and 100 μM serine
951 for 24 hours plotted against relative serine synthesis rates of cells cultured in corresponding
952 conditions. Serine synthesis rates are calculated from labeled serine (M+3) after 1 and 15 minutes
953 of U-^{13}C-glucose exposure and normalized to culture conditions with serine, n=3. Data shown are
954 means ± SD. P-values were calculated by unpaired Student's t-test, *p<0.05, **p<0.01,
955 ***p<0.001 ****p<0.0001, "ns" denotes not significant.
956
957 **Figure 4. Mitochondrial respiration governs the cell NAD+/NADH ratio and influences**
958 **serine synthesis. (A)** Schematic depicting the mitochondrial electron transport chain (ETC) and
959 the protonophore activity of FCCP that uncouples the ETC from ATP synthase activity. IMS,
960 intermembrane space; CoQ(H_2) indicates the oxidized and reduced (H_2) forms of coenzyme Q;
961 cyt_c, cytochrome c. **(B)** Proliferation rate (doublings per day) of A549 cells cultured with and
962 without serine with indicated concentrations of FCCP for 72 hours, n=3. **(C)** Proliferation rate
963 (doublings per day) of H1299 cells cultured with and without serine with indicated concentrations
964 of FCCP for 72 hours, n=3. **(D)** Serine labeled (M+3) from U-^{13}C-glucose over time in A549 cells
965 cultured without serine, and with and without 2 μM FCCP treatment for 24 hours prior to U-^{13}C-

966 glucose exposure. Serine levels are normalized to internal norvaline standard and cell number
967 measured in indicated conditions, n=3. **(E)** Serine labeled (M+3) from U-^{13}C-glucose over time in
968 H1299 cells cultured without serine, and with and without 2 μM FCCP treatment for 24 hours prior
969 to U-^{13}C-glucose exposure. Serine levels are normalized to internal norvaline standard and cell
970 number measured in indicated conditions, n=3. **(F)** Oxygen consumption rate (OCR) of A549 cells
971 cultured with and without serine with indicated FCCP treatment for 24 hours. Values are averages
972 of three repeat measurements, n=5-9. **(G)** Relative NAD+/NADH ratio of A549 cells cultured with
973 and without serine with indicated FCCP treatment for 24 hours. NAD+/NADH ratios are
974 normalized to the NAD+/NADH ratio in A549 cells culture with serine, n=3. **(H)** Proliferation rate
975 (doublings per day) of A549 cells cultured with and without serine, 2 μM FCCP, and indicated
976 concentrations of rotenone for 72 hours, n=3. **(I)** Serine labeled (M+3) from U-^{13}C-glucose over
977 time in A549 cells cultured without serine, and with and without 2 μM FCCP and 20 nM rotenone
978 as indicated, for 24 hours prior to U-^{13}C-glucose exposure. Serine levels are normalized to internal
979 norvaline standard and cell number measured in indicated conditions, n=3. **(J)** Relative
980 NAD+/NADH ratio of A549 cells cultured with and without serine, 2 μM FCCP, and 20 nM
981 rotenone as indicated. NAD+/NADH ratios are normalized to the NAD+/NADH ratio in untreated
982 A549 cells cultured with serine, n=3. Data shown are means ± SD. P-values were calculated by
983 unpaired Student's t-test, *p<0.05, **p<0.01, ***p<0.005, ****p<0.001, "ns" denotes not significant.
984

985 **Figure 5. Lipid depletion leads to a cell-specific elevation in mitochondrial respiration**
986 **and the NAD+/NADH ratio, influencing oxidative citrate and serine synthesis. (A)**
987 Schematic depicting glucose and glutamine oxidative routes for synthesizing citrate, highlighting
988 NAD+ requiring oxidation reactions. **(B)** Citrate labeled (M+2) from U-^{13}C-glucose over time in
989 H1299 and A549 cells cultured with and without serine for 24 hours prior to U-^{13}C-glucose
990 exposure. Citrate levels are normalized to internal norvaline standard and cell number
991 measured in indicated conditions, n=3. **(C)** Citrate labeled (M+2) from U-^{13}C-glucose over time

992 in A549 and H1299 cells cultured without serine, and with and without 2 μM FCCP for 24 hours
993 prior to U-^{13}C-glucose exposure. Citrate levels are normalized to internal norvaline standard and
994 cell number measured in indicated conditions, n=3. **(D)** Citrate labeled (M+2) from U-^{13}C-
995 glucose over time in A549 cells cultured with serine, and with indicated concentrations of AKB
996 or FCCP for 24 hours prior to U-^{13}C-glucose exposure. Citrate levels are normalized to internal
997 norvaline standard and cell number measured in indicated conditions, n=3. **(E)** Oxygen
998 consumption rate (OCR) in A549 and H1299 cells cultured with and without lipids for 24 hours.
999 Values are averages of three repeat measurements, n=10. **(F)** Relative NAD+/NADH ratios of
1000 A549 and H1299 cells cultured with and without lipids for 24 hours. NAD+/NADH ratios are
1001 normalized to the NAD+/NADH ratio of the corresponding cell type cultured with lipids, n=3. **(G)**
1002 Citrate labeled (M+2) from U-^{13}C-glucose over time in A549 and H1299 cells cultured with and
1003 without lipids for 24 hours prior to U-^{13}C-glucose exposure. Citrate levels are normalized to
1004 internal norvaline standard and cell number measured in indicated conditions, n=3. **(H)** Serine
1005 labeled (M+3) from U-^{13}C-glucose over time in A549 and H1299 cells cultured with and without
1006 lipids for 24 hours prior to U-^{13}C-glucose exposure. Serine levels are normalized to internal
1007 norvaline standard and cell number measured in indicated conditions, n=3. Data shown are
1008 means ± SD. P values were calculated by unpaired Student's t-test, *$p<0.05$.
1009

1010 **Figure 6. Lipid depletion increases mitochondrial respiration and the NAD+/NADH ratio in**
1011 **a cell specific manner to influence serine synthesis and proliferation in serine-depleted**
1012 **conditions. (A)** Oxygen consumption rate (OCR) of A549 and H1299 cells cultured with and
1013 without serine or lipids for 24 hours. Values are the average of three repeat measurements, n=14-
1014 15. **(B)** Relative NAD+/NADH ratios of A549 and H1299 cells culture with and without serine or
1015 lipids for 24 hours. NAD+/NADH ratio is normalized to the NAD+/NADH ratio in corresponding
1016 cell type cultured with serine and lipids, n=3. **(C, D)** Left: Serine labeled (M+3) from U-^{13}C-glucose
1017 over time in A549 cells (C) and H1299 cells (D) cultured without serine, and with or without lipids

1018 for 24 hours prior to U-^{13}C-glucose exposure. Right: Serine synthesis rates of A549 cells (C) and
1019 H1299 cells (D) cultured in conditions shown on left. Serine synthesis rates are calculated from
1020 labeled serine (M+3) after 1 and 15 minutes of U-^{13}C-glucose exposure and normalized to the
1021 serine synthesis rates of the corresponding cell type cultured without serine and with lipids. Serine
1022 levels are normalized to internal norvaline standard and cell number measured in indicated
1023 conditions, n=3. Single data point (H1299, -serine +lipid, t=15 min) removed due to error in sample
1024 processing. (**E,F)** Left: Citrate labeled (M+2) from U-^{13}C-glucose over time in A549 cells (E) and
1025 H1299 cells (F) cultured without lipids, and with or without serine for 24 hours prior to U-^{13}C-
1026 glucose exposure. Right: Citrate synthesis rates of A549 cells (E) and H1299 cells (F) cultured in
1027 conditions shown on left. Citrate synthesis rates are calculated from labeled citrate (M+2) after 1
1028 and 15 minutes of U-^{13}C-glucose exposure and normalized to the citrate synthesis rates of the
1029 corresponding cell type cultured without lipids and with serine. Citrate levels are normalized to
1030 internal norvaline standard and cell number measured in indicated conditions, n=3. **(G)**
1031 Proliferation rate (doublings per day) of A549 cells cultured with and without serine or lipids for 72
1032 hours, n=3. **(H)** Proliferation rate (doublings per day) of H1299 cells cultured with and without
1033 serine or lipids for 72 hours, n=3. Data shown are means ± SD. P-values were calculated by
1034 unpaired Student's t-test, *$p<0.05$ ***$p<0.005$. ****$p<0.001$.

Figure 1

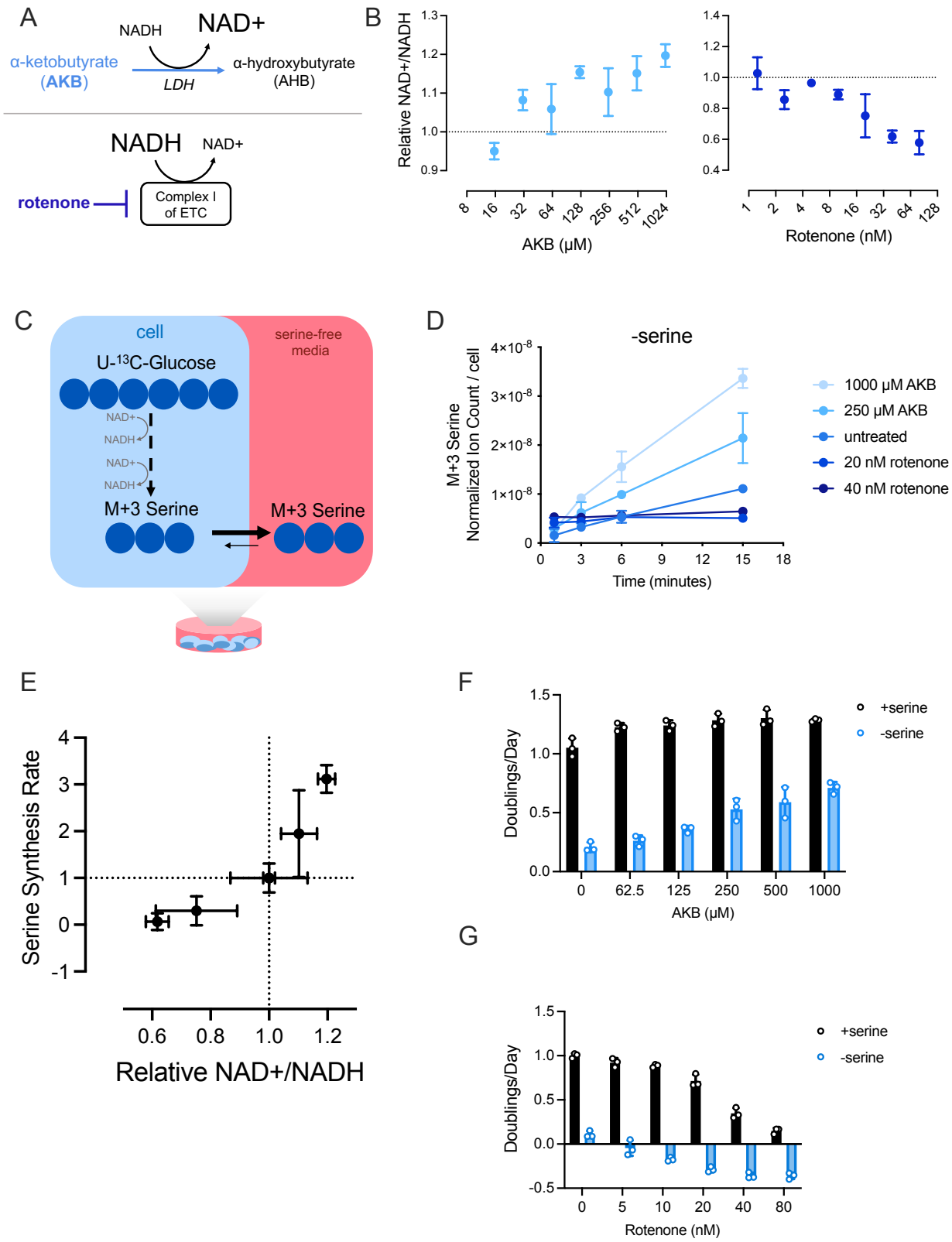
A
NADH
NAD+
α-ketobutyrate
(AKB)
LDH
α-hydroxybutyrate
(AHB)
NADH
NAD+
rotenone
Complex I
of ETC
B
Relative NAD+/NADH
AKB (μM)
Rotenone (nM)
C
cell
serine-free
media
U-13C-Glucose
NAD+
NADH
M+3 Serine
M+3 Serine
D
-serine
M+3 Serine
Normalized Ion Count / cell
Time (minutes)
1000 μM AKB
250 μM AKB
untreated
20 nM rotenone
40 nM rotenone
E
Serine Synthesis Rate
Relative NAD+/NADH
F
Doublings/Day
AKB (μM)
+serine
-serine
G
Doublings/Day
Rotenone (nM)
+serine
-serine

Figure 2

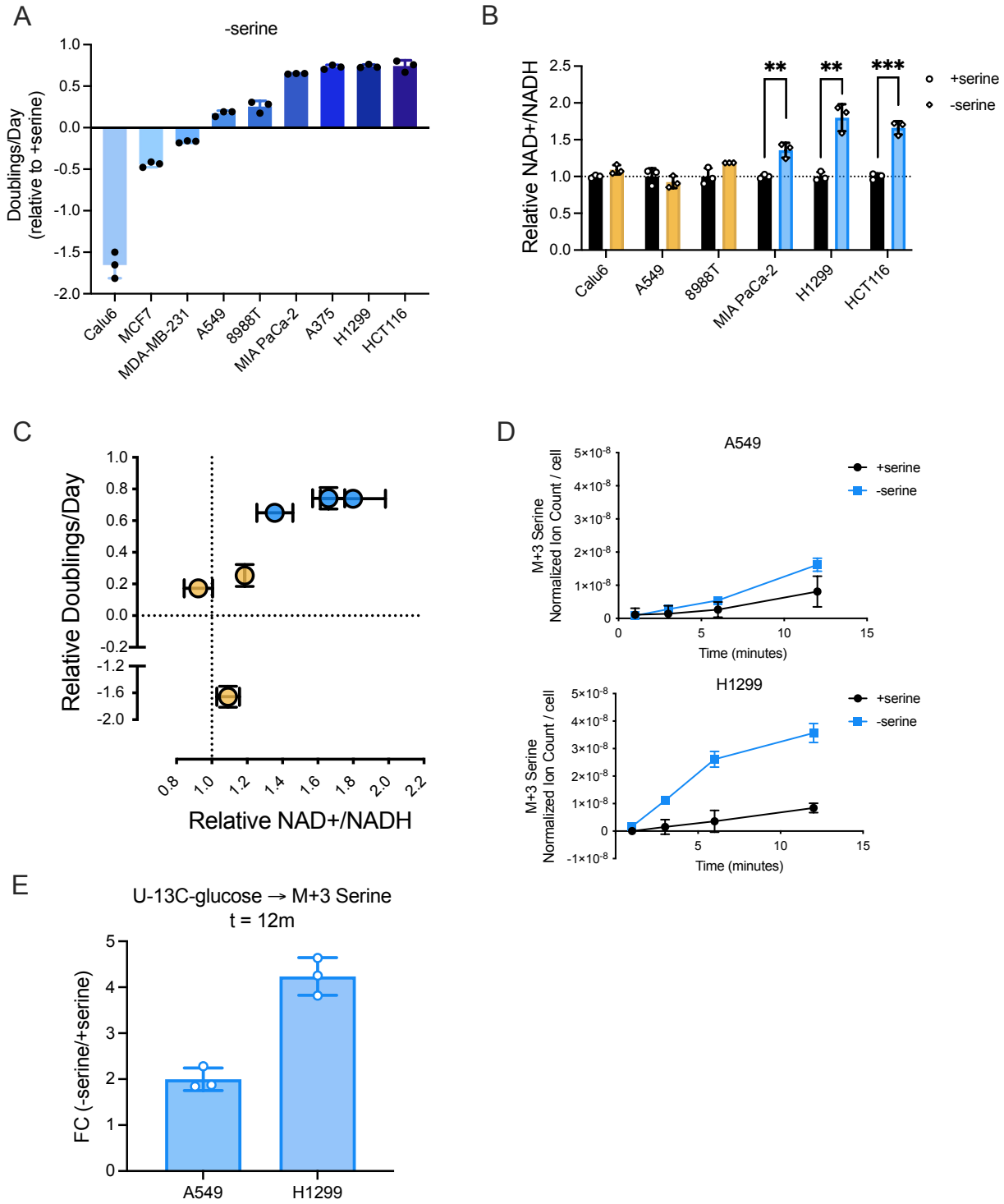
A
-serine
Doublings/Day
(relative to +serine)
1.0
0.5
0.0
-0.5
-1.0
-1.5
-2.0
Calu6
MCF7
MDA-MB-231
A549
8988T
MIA PaCa-2
A375
H1299
HCT116
B
Relative NAD+/NADH
2.5
2.0
1.5
1.0
0.5
0.0
**
**
***
+serine
-serine
Calu6
A549
8988T
MIA PaCa-2
H1299
HCT116
C
Relative Doublings/Day
1.0
0.8
0.6
0.4
0.2
0.0
-0.2
-1.2
-1.6
-2.0
0.8
1.0
1.2
1.4
1.6
1.8
2.0
2.2
Relative NAD+/NADH
D
A549
M+3 Serine
Normalized Ion Count / cell
5×10-8
4×10-8
3×10-8
2×10-8
1×10-8
0
0
5
10
15
Time (minutes)
+serine
-serine
H1299
M+3 Serine
Normalized Ion Count / cell
5×10-8
4×10-8
3×10-8
2×10-8
1×10-8
0
-1×10-8
5
10
15
Time (minutes)
+serine
-serine
E
U-13C-glucose → M+3 Serine
t = 12m
FC (-serine/+serine)
5
4
3
2
1
0
A549
H1299

Figure 3

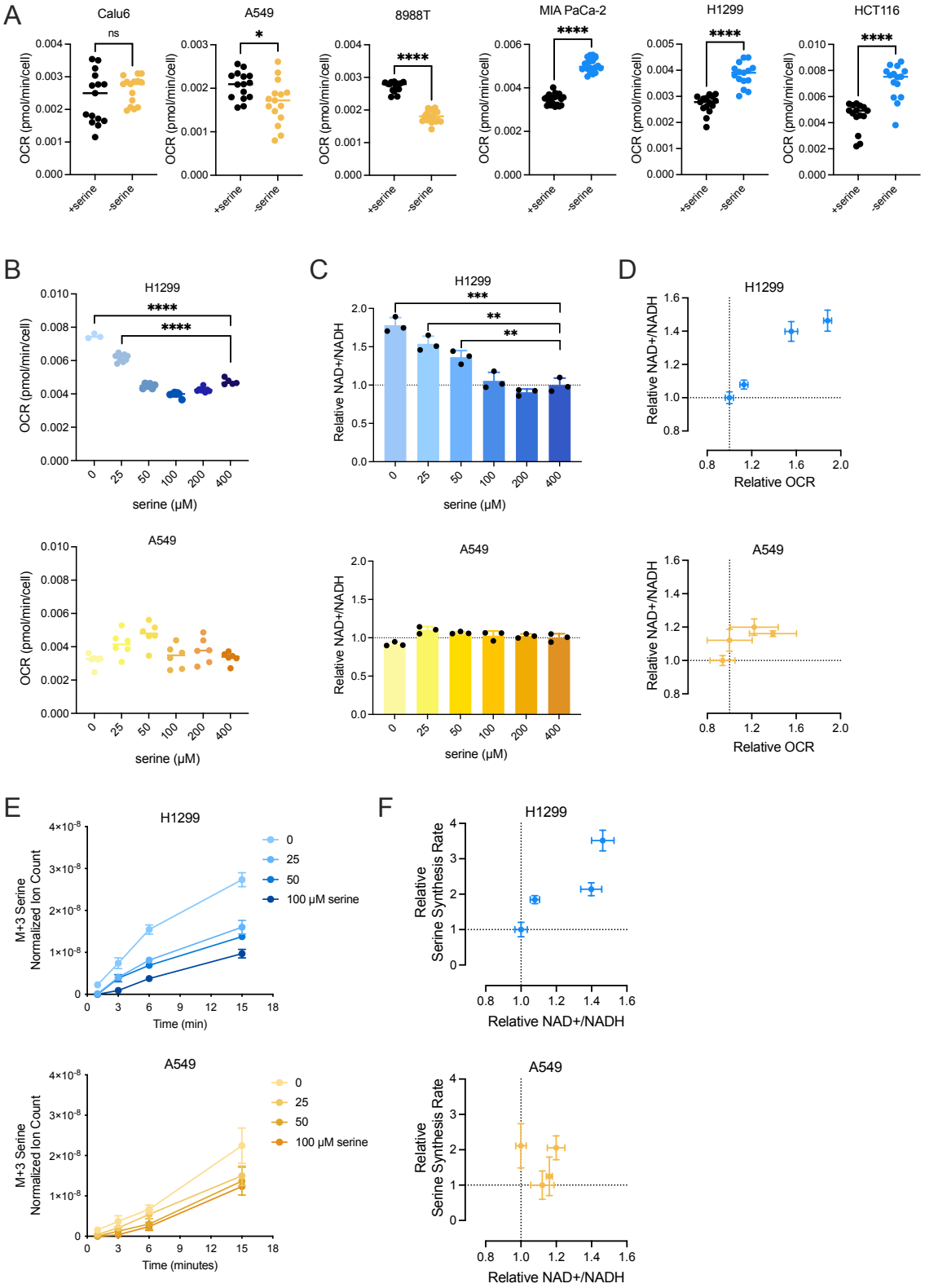
A
Calu6
A549
8988T
MIA PaCa-2
H1299
HCT116
OCR (pmol/min/cell)
ns
*
****
+serine
-serine
B
H1299
A549
serine (μM)
C
Relative NAD+/NADH
***
**
D
Relative OCR
E
M+3 Serine Normalized Ion Count
Time (min)
Time (minutes)
0
25
50
100 μM serine
F
Relative Serine Synthesis Rate
Relative NAD+/NADH

Figure 4

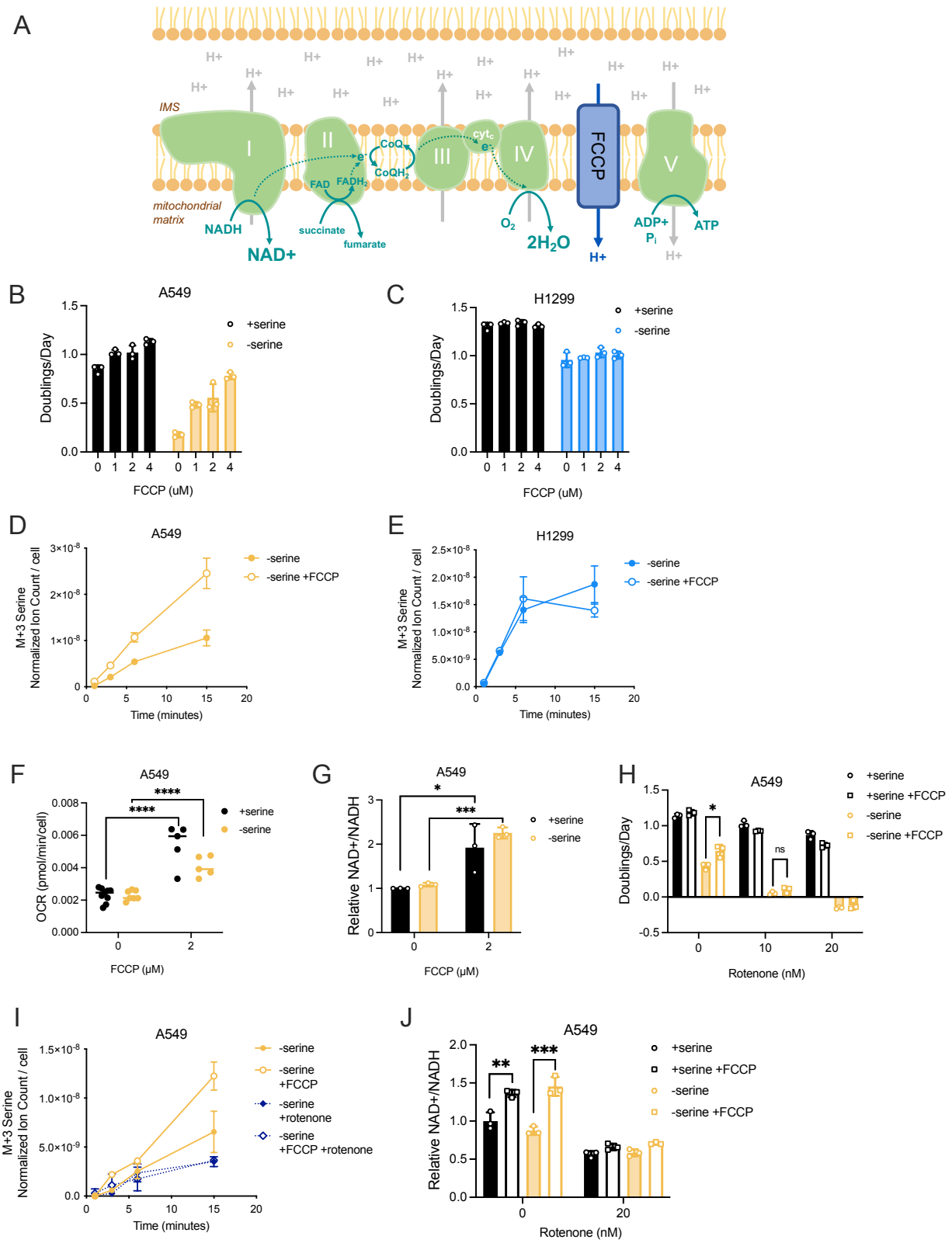
A
IMS
mitochondrial matrix
I
II
III
IV
V
FCCP
NADH
NAD+
succinate
fumarate
FAD
FADH2
CoQ
CoQH2
cytc
O2
2H2O
ADP+ Pi
ATP
H+
B
A549
Doublings/Day
+serine
-serine
FCCP (uM)
C
H1299
Doublings/Day
+serine
-serine
FCCP (uM)
D
A549
M+3 Serine Normalized Ion Count / cell
-serine
-serine +FCCP
Time (minutes)
E
H1299
M+3 Serine Normalized Ion Count / cell
-serine
-serine +FCCP
Time (minutes)
F
A549
OCR (pmol/min/cell)
****
****
+serine
-serine
FCCP (μM)
G
A549
Relative NAD+/NADH
*
***
+serine
-serine
FCCP (μM)
H
A549
Doublings/Day
*
ns
+serine
+serine +FCCP
-serine
-serine +FCCP
Rotenone (nM)
I
A549
M+3 Serine Normalized Ion Count / cell
-serine
-serine +FCCP
-serine +rotenone
-serine +FCCP +rotenone
Time (minutes)
J
A549
Relative NAD+/NADH
**
***
+serine
+serine +FCCP
-serine
-serine +FCCP
Rotenone (nM)

Figure 5

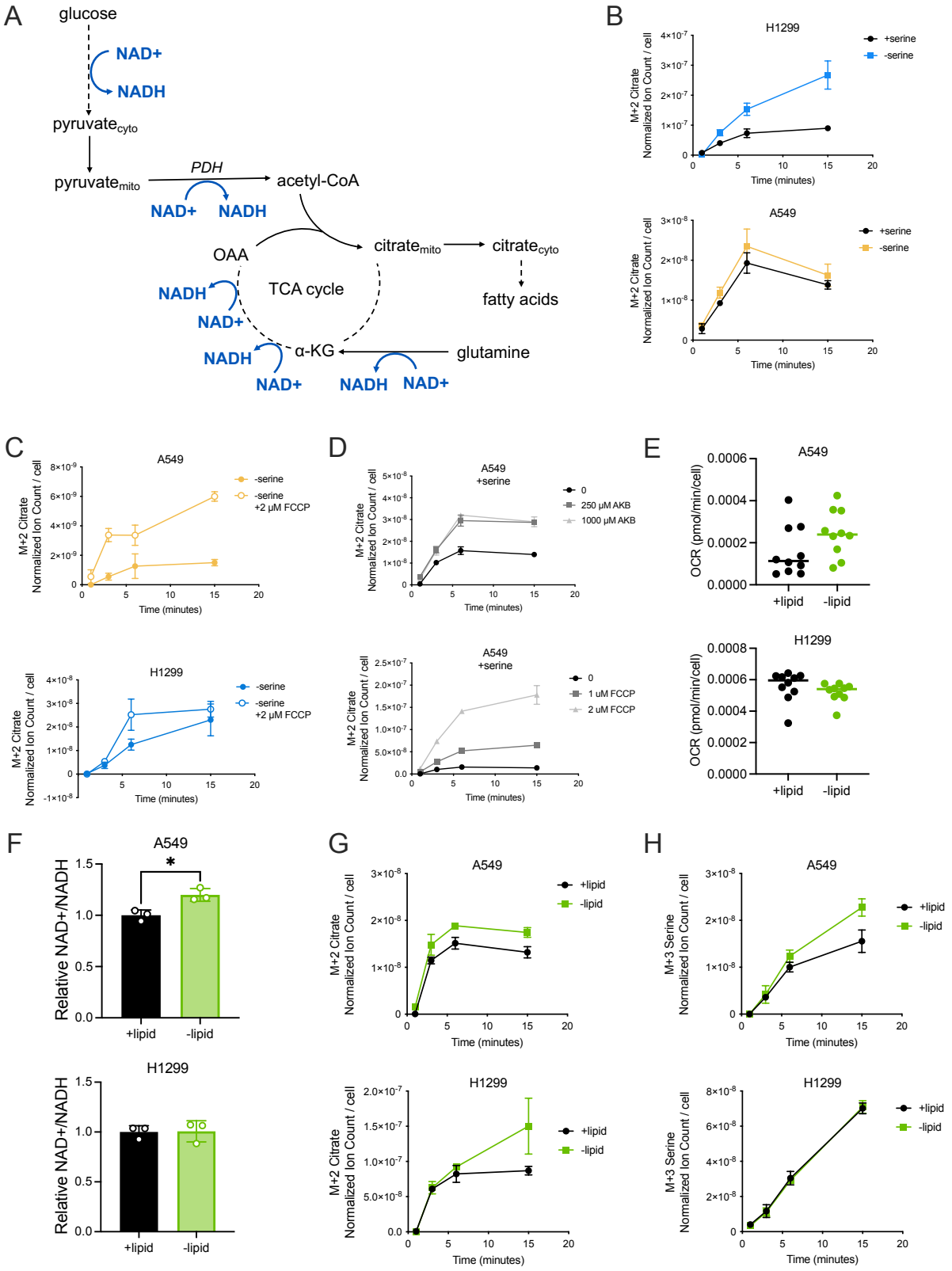
A
glucose
NAD+
NADH
pyruvate$_{cyto}$
pyruvate$_{mito}$
PDH
NAD+
NADH
acetyl-CoA
OAA
citrate$_{mito}$
citrate$_{cyto}$
TCA cycle
fatty acids
NADH
NAD+
NADH
NAD+
α-KG
glutamine
NAD+
NADH
B
H1299
A549
+serine
-serine
M+2 Citrate Normalized Ion Count / cell
Time (minutes)
C
A549
H1299
-serine
-serine +2 μM FCCP
D
A549 +serine
0
250 μM AKB
1000 μM AKB
1 uM FCCP
2 uM FCCP
E
A549
H1299
OCR (pmol/min/cell)
+lipid
-lipid
F
A549
H1299
Relative NAD+/NADH
G
H
M+3 Serine Normalized Ion Count / cell

Figure 6

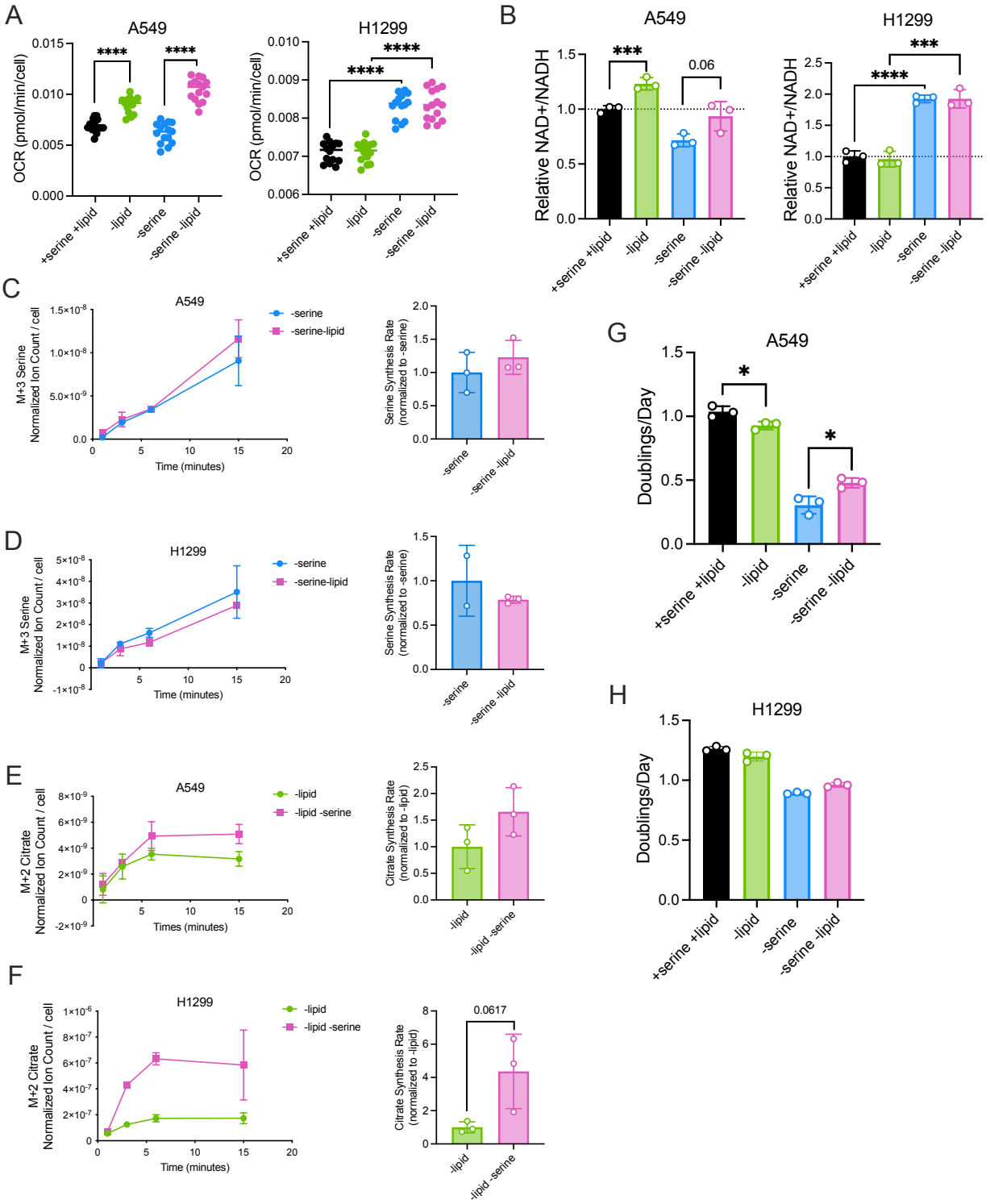
A
A549
H1299
OCR (pmol/min/cell)
****
+serine +lipid
-lipid
-serine
-serine -lipid
B
Relative NAD+/NADH
***
0.06
C
M+3 Serine Normalized Ion Count / cell
Time (minutes)
-serine
-serine-lipid
Serine Synthesis Rate (normalized to -serine)
D
E
M+2 Citrate Normalized Ion Count / cell
Times (minutes)
-lipid
-lipid -serine
Citrate Synthesis Rate (normalized to -lipid)
F
0.0617
G
Doublings/Day
*
H